

Evidence for geomagnetic excursions recorded in Brunhes and Matuyama Chron lavas from the trans-Mexican volcanic belt

Daniel M. Michalk,^{1,5} Harald N. Böhnel,² Norbert R. Nowaczyk,¹ Gerardo J. Aguirre-Díaz,² Margarita López-Martínez,³ Steven Ownby,⁴ and Jörg F. W. Negendank¹

Received 3 December 2012; revised 3 May 2013; accepted 6 May 2013; published 14 June 2013.

[1] This study presents paleomagnetic data from 59 independent lava flows from the trans-Mexican volcanic belt (TMVB) with ages from 6.4 Ma to recent, 52 being younger than 1 Ma, and 11 new ⁴⁰Ar/³⁹Ar age determinations. Most remanence carriers are Ti-poor titanomagnetite of pseudosingle-domain magnetic structure, nine lavas contain small amounts of titanomaghemite, and four lavas additional (titano-) hematite. Paleosecular variation of lava flows younger than 1.7 Ma is consistent with latitude-dependent Model G and also in agreement with other Pleistocene paleomagnetic data from the TMVB. The directional record of Brunhes and Matuyama Chrons lavas was correlated to the geomagnetic polarity timescale and there is evidence for at least four geomagnetic excursions. One lava flow dated at 592 ± 20 ka has a fully reversed paleodirection and most likely erupted during the Big Lost excursion. Another fully reversed flow, dated at 671 ± 12 ka, gives new volcanic evidence for the Delta/Stage 17 excursion. This excursion is supported by a reversed intermediate direction of another flow from a different volcanic field but of very close age of 673 ± 10 ka. From the Matuyama age lavas, one flow with normal polarity magnetization, dated at 949 ± 37 ka, could either be related to the Kamikatsura or the Santa Rosa excursion and a normal polarity flow, dated at 1628 ± 56 ka, could have been emplaced during the Gilsa excursion. The results presented here confirm in one case but disagree in four cases with results presented in two previous studies of the same lava flows and interpreted as geomagnetic excursions.

Citation: Michalk, D. M., H. N. Böhnel, N. R. Nowaczyk, G. J. Aguirre-Díaz, M. López-Martínez, S. Ownby, and J. F. W. Negendank (2013), Evidence for geomagnetic excursions recorded in Brunhes and Matuyama Chron lavas from the trans-Mexican volcanic belt, *J. Geophys. Res. Solid Earth*, 118, 2648–2669, doi:10.1002/jgrb.50214.

1. Introduction

[2] It is known since *Brunhes* [1906] that the Earth's magnetic field switches polarity, and from the geological record, it is known that complete polarity field reversals have occurred intermittently through geological time [*Cande and Kent*, 1992, 1995]. The last geomagnetic reversal occurred 776 ± 2 ka ago [*Coe et al.*, 2004; *Singer et al.*, 2005] when

it changed from a reversed polarity regime (Matuyama Chron, 0.78–2.56 Ma) to its present normal polarity regime (Brunhes Chron). During these Chrons, the magnetic field departed several times from its predominant axial dipole configuration, as indicated by numerous geomagnetic excursions and events reported in the literature [e.g., *Champion et al.*, 1988; *Langereis et al.*, 1997; *Lund et al.*, 1998, 2006; *Singer et al.*, 1999, 2002, 2008a, 2008b]. Geomagnetic excursions can be defined as relatively short periods within an otherwise stable polarity chron, during which the field directions lie outside the range of expected secular variation of the geocentric axial dipole (GAD) field configuration. In the case of a geomagnetic excursion, the field returns after a few thousand years to the same polarity, whereas in the case of a geomagnetic event, the field reverses completely for a short time. Depending on the particular excursion and the location on the globe of the rocks that recorded them, geomagnetic excursions/events may last for ~2 ka up to ~10 ka, making their identification difficult not only in marine and lacustrine sediments with low deposition rates but also in volcanic rocks that are only extruded sporadically. There is still a considerable debate about the number of true excursions with potentially up to 17 excursions within the Brunhes Chron alone [*Lund et al.*, 2006] and up to nine

Additional supporting information may be found in the online version of this article.

¹Helmholtz-Zentrum Potsdam, Deutsches GeoForschungsZentrum, Potsdam, Germany.

²Centro de Geociencias, Universidad Nacional Autónoma de México, Juriquilla, Mexico.

³División de Ciencias de la Tierra, Centro de Investigación Científica y de Educación Superior de Ensenada, Ensenada, Mexico.

⁴Department of Geological Sciences, University of Michigan, Ann Arbor, Michigan, USA.

⁵Statoil, Emden, Germany.

Corresponding author: H. N. Böhnel, Centro de Geociencias, Universidad Nacional Autónoma de México, Blvd. Juriquilla 3001, Juriquilla, Queretaro 76230, Mexico. (hboehnel@geociencias.unam.mx)

©2013. American Geophysical Union. All Rights Reserved.
2169-9313/13/10.1002/jgrb.50214

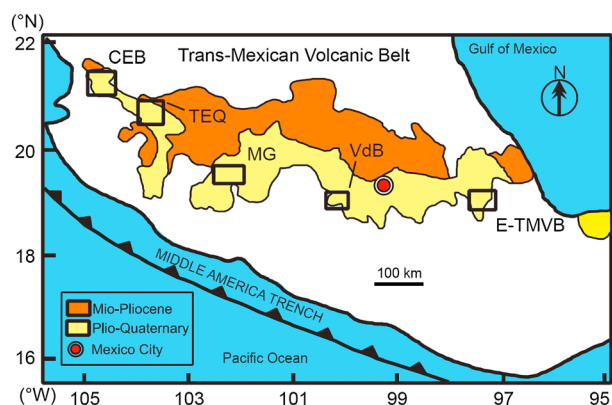


Figure 1. Schematic map of the trans-Mexican volcanic belt showing the sampling areas indicated by solid rectangles. CEB=Ceboruco San-Pedro volcanic field, TEQ=Tequila volcanic field, MG=Michoacan Guanajuato volcanic field, VdB=Valle de Bravo volcanic field, E-TMVB=eastern trans-Mexican volcanic belt (modified after *Aguirre-Díaz* [1996]).

within the reverse Matuyama Chron [*Channell et al.*, 2002]. These numbers should be considered as upper limits though.

[3] Excursions are generally accompanied with intensity lows as documented in relative paleo-intensity records from marine sediment cores [see *Lund et al.*, 2006, and references therein], but little is known about the primary geodynamic processes that lead to a geomagnetic excursion as well as the total duration of an excursion. *Doell and Cox* [1972] and *Opdyke* [1972] suggested that a geomagnetic excursion represents an incomplete polarity transition (aborted reversal) before the field returns back to a stable polarity state. More recently, *Gubbins* [1999] proposed that excursions reflect shorter and more frequent weakenings of the main dipole field where the field reverses only in the liquid outer core, on short timescales of around 500 years, but not in the solid inner core, where the diffusion time of magnetic flux must exceed about 3 ka in order to maintain a full reversal for a longer time. This hypothesis has been challenged by *Knudsen et al.* [2007], who presented evidence that the field spends around 7 to 8 ka in a transitional state (including virtual geomagnetic poles (VGPs) reaching high southerly latitudes), which is a similar time span to the estimated duration of a polarity reversal [*Clement*, 2004]. Numerical dynamo simulations by *Wicht* [2005] suggest a strong site dependence on the occurrence and duration of excursions, which means that many excursions might not be a global feature of the geomagnetic field. There is little knowledge about the timing, duration, and global validity of excursions, but it is now assumed by many workers that during the Brunhes Chron and perhaps the Matuyama Chron, the geodynamo was characterized by up to 20% of the time by a weak non-dipole state [e.g., *Merrill and McFadden*, 1994; *Guyodo and Valet*, 1999], and it is likely that this was true for other polarity chrons as well. Therefore, knowing the precise number of geomagnetic excursions, their timing, and duration, and recognizing them in different parts of the globe are essential for a more complete understanding of the complex dynamo processes. Up to the present, volcanic evidence exists for nine excursions within the Brunhes Chron (Laschamp, possibly Norwegian-Greenland

Sea, Blake, Pringle Falls, Calabrian Ridge 2/West Eifel 5, West Eifel 4, Big Lost/West Eifel 3, West Eifel 2, and West Eifel 1) and six within the Matuyama (Kamikatsura, Santa Rosa, Punaruu, Cobb Mountain, Gilsa, and Réunion) [see *Singer et al.*, 2002, 2004; *Singer*, 2007; *Singer et al.*, 2008a, 2008b]. Yet, for an unambiguous confirmation of excursions records from sediments and their global validity, more evidence from radioisotopically dated volcanic rocks is highly desired. If ages are well constrained, they provide geochronologic tie points for calibrating the global record of relative paleo-intensity and associated distortions of its geometry.

[4] We report a detailed integrated rock and paleomagnetic study of 64 independent lava flows with radioisotopically constrained ages from recent back to 6.4 Ma from within the trans-Mexican volcanic belt (TMVB). New age data were determined for 11 lavas using the $^{40}\text{Ar}/^{39}\text{Ar}$ method. The main objective was to identify, if possible, some of the geomagnetic excursions within the Brunhes and Matuyama Chrons in order to contribute to the geomagnetic instability timescale [*Singer et al.*, 2002, 2008a, 2008b].

2. Geological Setting

[5] The target of the present study was the E-W trending TMVB, which crosses central Mexico from coast to coast at latitudes from 19 to 21°N with a width between 20 and 150 km (Figure 1). Nearly 1000 km long, it is one of the largest continental volcanic arcs on the North American Plate. Its western part is associated with the subduction of the Rivera Plate (commencing at ~9 Ma), whereas the eastern part relates to the subduction of the Cocos Plate (commencing at 12–18 Ma) under the North American Plate (middle American Trench) [*Klitgord and Mammerickx*, 1982]. The TMVB comprises roughly 8000 volcanic structures, mainly stratovolcanoes, cinder cones, and caldera complexes, with probably many hundreds of them being younger than 2 Ma [e.g., *Demant*, 1978; *Aguirre-Díaz et al.*, 1998].

[6] Four monogenic volcanic fields have been reported in the TMVB [*Aguirre-Díaz et al.*, 2006]: Michoacán-Guanajuato, Jilotepec, Chichinautzin, and Valle de Bravo. Paleomagnetic sampling was carried out in two of them, Michoacán-Guanajuato and Valle de Bravo, and in other localities relevant for this study. In summary, samples were collected at (1) Ceboruco-San Pedro (CEB), (2) Tequila (TEQ), (3) Michoacan-Guanajuato (MG), and (4) Valle de Bravo (VdB) volcanic fields, and (5) Cofre de Perote-Pico de Orizaba at the eastern part of the TMVB (hereafter referred to as E-TMVB). Our criteria in the selection of the sampling sites were (1) the availability of reliable radioisotopic age determinations from previous geochronological studies and (2) a representative coverage of the TMVB from west to east.

3. Geochronology

[7] The majority of lavas were previously dated by the $^{40}\text{Ar}/^{39}\text{Ar}$ method, and details of the methodology used are found in *Blatter et al.* [2001], *Frey et al.* [2004], *Lewis-Kenedi et al.* [2005], and *Ownby et al.* [2007, 2011]. All ages used below are given with 1 σ error limits. These ages were reported relative to Fish Canyon Tuff biotite of 27.99 ± 0.04 Ma, apart from *Blatter et al.* [2001], who used

Fish Canyon Tuff sanidine of 28.02 Ma. Carrasco-Núñez *et al.* [2007, 2010] and Ort and Carrasco-Núñez [2009] reported three ages used in this work, but not much detail about the geochronology experiments is available. Nevertheless, these data are used here only to restrict the ages of these lava flows to the Brunhes Chron. Three further rocks were dated using thermoluminescence (TL) methods on quartz separates [Schaaf and Ramírez-Luna, 2008]. In the course of the present study, 11 new $^{40}\text{Ar}/^{39}\text{Ar}$ ages of lava flows from the VdB were determined at Centro de Investigación Científica y de Educación Superior de Ensenada (CICESE), Ensenada, Mexico. Complete details of the methodology are given in the supporting information, where we also include the age spectra, $^{37}\text{Ar}_{\text{Ca}}/^{39}\text{Ar}_{\text{K}}$ diagrams, $^{36}\text{Ar}/^{40}\text{Ar}$ versus $^{39}\text{Ar}/^{40}\text{Ar}$ correlation diagrams, and tables with all the relevant ^{40}Ar - ^{39}Ar information of the experiments performed. Whole rock and groundmass samples were analyzed. The majority of the samples were analyzed with a VG5400 mass spectrometer. For these experiments, a Coherent Innova 70 argon laser was used to release the argon isotopes. Two samples were analyzed with the MS-10 mass spectrometer which uses a temperature-controlled Ta furnace to heat the samples. For these experiments, aliquots of 1 to 2 g of sample were used to compensate for the low sensitivity of the MS-10 mass spectrometer. To test the reproducibility of the experiments, two samples were analyzed using both mass spectrometers. The argon isotopes were corrected for blank, mass discrimination, neutron-induced interference reactions, and radioactive decay of ^{37}Ar and ^{39}Ar . Irradiation monitors used were sanidine TCR (28.34 ± 0.28 Ma) [Renne *et al.*, 1998], biotite HD B1 (24.18 ± 0.09 Ma) [Schwarz and Trieloff, 2007], and CICESE's internal standard biotite CATAV 7-4 (89.13 ± 0.35 Ma). The constants recommended by Steiger and Jäger [1977] were used in all the calculations, while all the straight-line calculations were performed with the equations presented in York *et al.* [2004]. All errors are reported at 1σ level. Plateau ages were calculated with the weighted mean of three or more consecutive fractions which were in agreement within 1σ errors and where the sum of the ^{39}Ar released in these fractions was greater than 50%. All the data were plotted in the $^{36}\text{Ar}/^{40}\text{Ar}$ versus $^{39}\text{Ar}/^{40}\text{Ar}$ diagram to determine the composition of the ($^{40}\text{Ar}/^{36}\text{Ar}$)_{*i*} of the samples; however, some samples were characterized by poor ^{40}Ar radiogenic content, and therefore, the data distribution in the correlation diagram did not yield well-defined straight lines. Such behavior did not permit the calculation of reliable isochron ages, and in these cases, the plateau ages were taken as the best estimate for the cooling age of the lavas.

4. Previous Paleomagnetic Studies

[8] The TMVB has been the target of numerous paleomagnetic studies since the 1970s. The earliest studies [e.g., Mooser *et al.*, 1974] were primarily carried out for magnetostratigraphic purposes, while several subsequent studies were concerned with the tectonic evolution or for studying the paleosecular variation (PSV) [e.g., Herrero-Bervera and Pal, 1977; Böhnell and Negendank, 1981; Steele, 1985; Herrero-Bervera *et al.*, 1986]. Later studies focused on studying the PSV and absolute paleo-intensity (PI) on lava flows younger than 40 ka [Gonzalez *et al.*,

1997; Morales *et al.*, 2001; Böhnell and Molina-Garza, 2002]. Böhnell and Molina-Garza [2002] presented a compilation of PSV and PI data from Mexico covering the last 40 ka. Another comprehensive compilation of PSV data ranging from Pleistocene to recent age is presented by Mejía *et al.* [2005], who applied a strict quality index to previously published paleomagnetic data. These data indicate values of PSV for Mexico that are consistent with latitude-dependent Model G of McFadden *et al.* [1988, 1991] and a time-averaged field, which is best described by an axial geocentric dipole plus a 5% quadrupole contribution. More recently, two studies were published with evidence that some Brunhes Chron lava flows from Mexico recorded geomagnetic excursions. Petronille *et al.* [2005] reported results from three lavas with intermediate to fully reversed directions being contemporary with the Big Lost excursion [Champion *et al.*, 1988] and the Brunhes/Matuyama precursor [Singer *et al.*, 2005]. Ceja *et al.* [2006] linked three lavas with intermediate to reversed magnetizations to the Levantine excursion [Ryan, 1972; Biswas *et al.*, 1999] and the Delta excursion [Creer *et al.*, 1980], respectively.

5. Paleomagnetic Sampling and Experimental Techniques

[9] Sampling sites were selected according to the available geochronology data. In case of the rocks dated as part of the present study, sites were, of course, identical for both methods, while for previously published age data, we used the GPS coordinates included in the respective publications. Paleomagnetic site coordinates sometimes differ slightly from geochronology site coordinates, as only rocks that are believed to be *in situ* may be sampled. This is not a stringent requirement for geochronology sampling, e.g., in the case of blocky lava flows. As described below, there are contradictions between the paleomagnetic results presented here and other data reported previously for the same alleged sites. After learning about these contradictions, we revised the flow extension on air photographs and Google Earth images and went back to the field to check if our sites indeed corresponded to the rock units that were dated, and we are confident that our paleomagnetic results indeed do so. In some cases, we could confirm the location of the previous sampling by Petronille *et al.* [2005] and Ceja *et al.* [2006] by identifying the drill holes, but in other cases, this was not possible using the published coordinates.

[10] Volcanic rocks were sampled using drill bits of 12 mm diameter, which yielded the so-called "mini-core" samples. Drill cores of that size have been shown to produce similar paleomagnetic data compared to 25 mm drill cores as used traditionally [Böhnell *et al.*, 2009]. The 12 mm cores were selected as they offered advantages for paleo-intensity experiments [Michalk *et al.*, 2008]. Paleomagnetic samples were distributed across an outcrop interval as much as possible, in general, more than 15 m, to avoid biased site mean directions due to individual moved blocks. Cores were oriented with magnetic and Sun compasses. We sampled only fresh outcrops that showed no apparent signs of alteration due to weathering. Later, drill cores were cut into four to five specimens of 10 mm length.

[11] The natural remanent magnetization (NRM) of 5–21 specimens, one per drill core, from each flow was

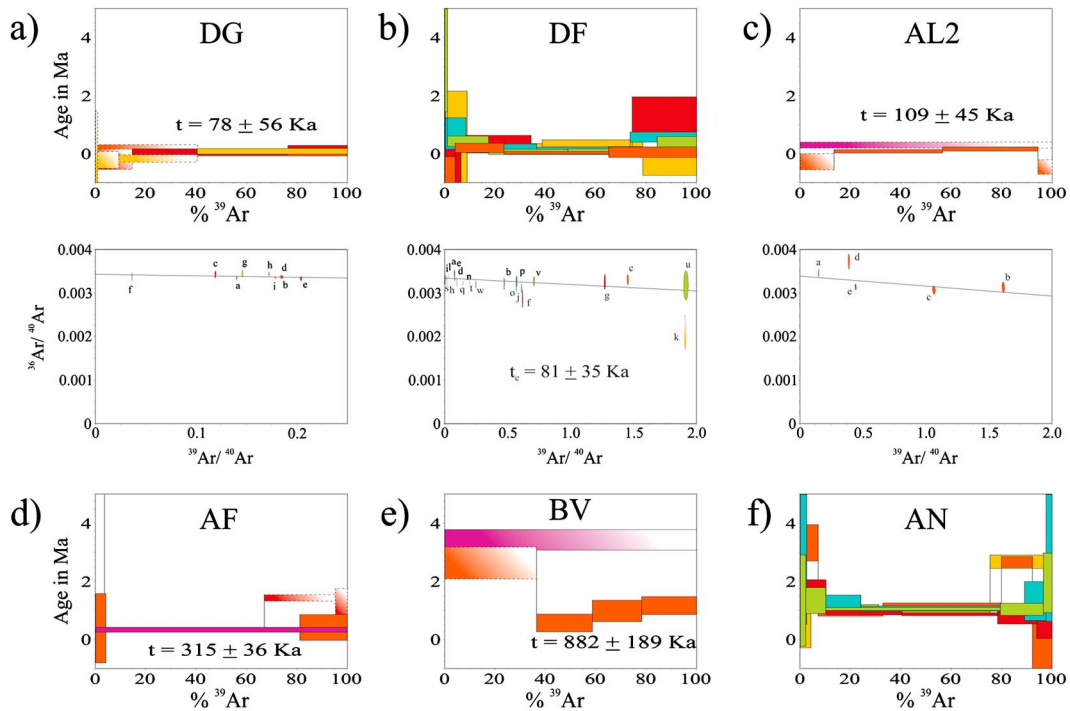


Figure 2. Age spectra and $^{36}\text{Ar}/^{40}\text{Ar}$ versus $^{39}\text{Ar}/^{40}\text{Ar}$ correlation diagram for the samples as identified by sites codes (see Table 2). Preferred ages are indicated in the diagrams. The fractions selected to calculate the weighted mean ages are displayed in the age spectra with solid color. Otherwise, the preferred isochron age is given in the correlation diagrams. Data ignored in the calculation are plotted with dashed line and graded color. To facilitate the comparison of the age results, the age spectra were plotted in the same scale. For the correlation diagrams, different scales were selected to highlight the distribution of the data. The Ta furnace step-heating, laser step-heating, and laser one-step experiments are shown in by different colors, as given in the right bottom corner.

measured using a cryogenic magnetometer (2G Enterprises 755 SRM) with long core setup at the Deutsches GeoForschungsZentrum. The only exception was site DH, from which only three oriented cores were available. Stepwise alternating field (AF) demagnetization was carried out fully automatically with the in-line three-axis AF demagnetizer over 10 or 11 demagnetization steps with peak fields up to 125 mT, while thermal demagnetization was applied to a smaller subset of samples (two to four samples per flow) over 11 to 13 demagnetization steps, using a Magnetic Measurements Ltd. model MMTD oven. After each thermal demagnetization step, low-field magnetic susceptibility (χ) was measured with a Bartington MS2B susceptibility sensor to monitor possible chemical alterations during heating.

[12] A combination of rock magnetic measurements was performed on selected samples to confidently ascertain the magnetic mineralogy and grain size, as well as the mechanisms by which this remanence was acquired. Thermomagnetic curves (M_s - T curves) were measured on two samples per flow, with a variable field translation balance (VFTB) from room temperature to 600–700°C in an argon environment, applying a field of 500 mT. Curie temperatures (T_C) were then determined after the method of Moskowitz [1981]. Sets of two to three hysteresis measurements, backfield, and isothermal remanent magnetization (IRM) acquisition curves were measured on 30–50 mg rock chips with a Princeton Measurements model Micromag 2900 Alternating Field Gradient Magnetometer (AGFM). From

those data (after the removal of the paramagnetic contribution), the standard hysteresis parameters were determined: the saturation magnetization (M_S), the saturation remanence (M_{RS}), the coercivity force (B_C), and the coercivity of remanence (B_{CR}). Using the ratios M_{RS}/M_S and B_{CR}/B_C , a Day plot was created [Day *et al.*, 1977, Dunlop, 2002] to deduce the bulk magnetic domain state. The S ratio [Bloemendal *et al.*, 1992] was also determined. Polished sections from one sample per flow were prepared for ore microscopy studies, which were carried out using a reflected light microscope and a Zeiss DSM962 scanning electron microscope.

6. Results

6.1. ^{40}Ar - ^{39}Ar Geochronology

[13] The results obtained for the 11 samples dated are summarized in Figure 2 and listed in Table 1, and the preferred age for each sample is indicated either on the age spectrum or in the correlation diagram. Site codes correspond to Table 2.

[14] Site DG: Three laser step-heating experiments were performed on groundmass fragments from the sample. The two, three, and four fractions collected respectively on the step-heating experiments yielded reproducible results. Because the sample is characterized by low $^{40}\text{Ar}^*$ content, the data plot is very close to the ordinate axis of the $^{36}\text{Ar}/^{40}\text{Ar}$ versus $^{39}\text{Ar}/^{40}\text{Ar}$ correlation diagram and therefore

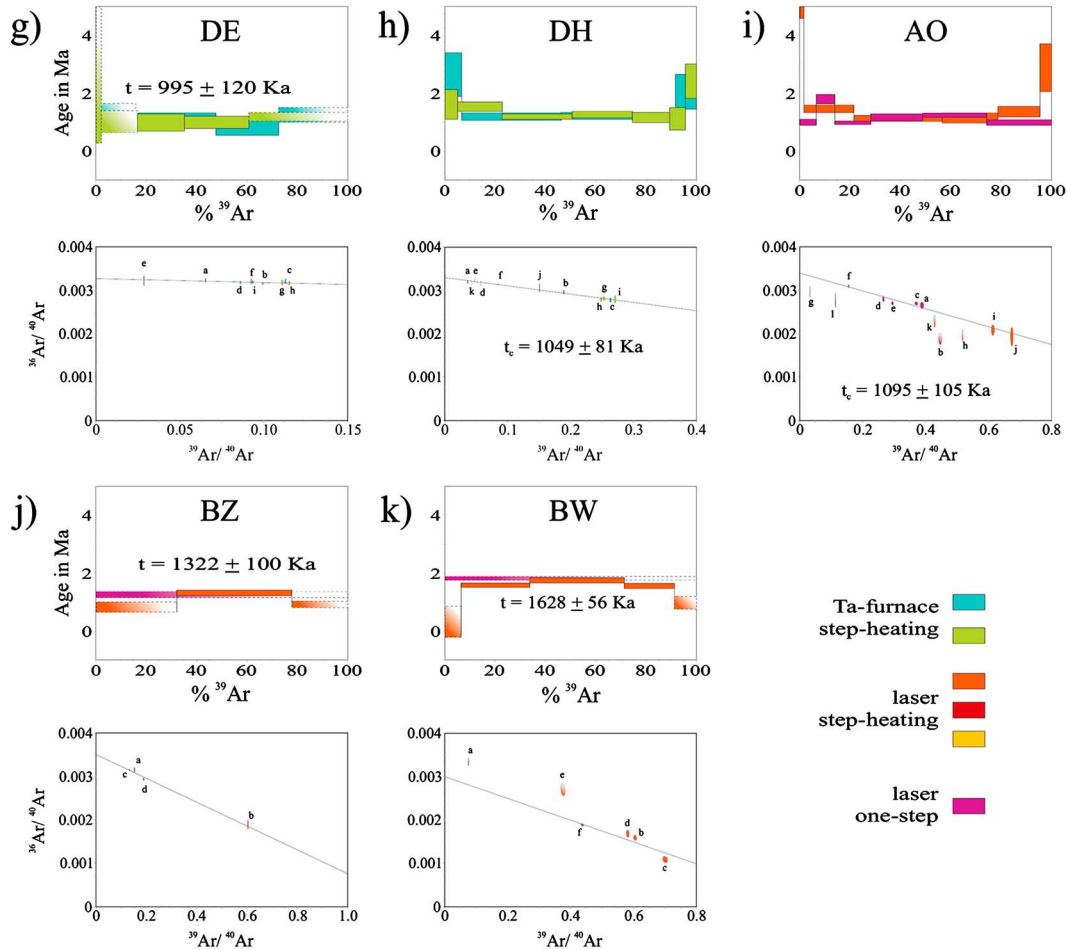


Figure 2. (continued)

does not constrain a reliable isochron age. The preferred age of $78 \pm 56 \text{ ka}$ was obtained from the mean square of weighted deviation ($\text{MSWD} = 0.11$) of the four fractions that represent the bulk of the ^{39}Ar (these are identified by solid boxes in Figure 2a).

[15] Site DF: Three step-heating experiments with the laser, plus two step-heating experiments with the temperature-controlled Ta furnace were performed with a whole rock sample. The age spectra obtained (see Figure 2b) indicate reproducible results. A slight saddle shape is displayed in the age spectra. The fractions released at intermediate temperatures cluster about 80 ka. The data from the five step-heating experiments performed define a straight line ($\text{MSWD} = 1.36$ for $n = 22$) in the $^{36}\text{Ar}/^{40}\text{Ar}$ versus $^{39}\text{Ar}/^{40}\text{Ar}$ correlation diagram. The isochron age of $81 \pm 35 \text{ ka}$ is the preferred age for this sample.

[16] Site AL2: The results obtained with a whole rock sample are shown in Figure 2c. Two laser experiments were performed, a one-step fusion and a step-heating run. The sample yielded low $^{40}\text{Ar}^*$. In the step-heating experiment, the bulk of the ^{39}Ar (81%) was released in two fractions. The age calculated from their weighted mean is $109 \pm 45 \text{ ka}$, which is the preferred age for this sample. Furthermore, the isochron age of $122 \pm 94 \text{ ka}$ calculated with all the data points is statistically indistinguishable from the weighted mean result.

[17] Site AF: Two laser step-heating experiments and a one-step fusion were performed with a groundmass sample. The

results are presented in Figure 2d. The sample composition was not homogeneous with respect to the radiogenic argon content. The first step-heating experiment yielded ages clustering at $\sim 300 \text{ ka}$ in agreement with the age of $330 \pm 83 \text{ ka}$ obtained from the one-step laser fusion experiment. The second experiment displays a pronounced saddle-shaped age spectra. More than 60% of the ^{39}Ar was released in the second fraction, which yielded a $309 \pm 49 \text{ ka}$ age. The data do not constrain an isochron age; however, the line calculated with all the data is in agreement with the $\sim 300 \text{ ka}$ age. The preferred age of $315 \pm 36 \text{ ka}$ was obtained as the weighted mean of five fractions ($\text{MSWD} = 0.02$) (fractions selected are displayed in solid color in the age spectrum in Figure 2d).

[18] Site BV: A laser step-heating experiment and a laser one-step fusion were performed for the groundmass fragments (Figure 2e). The ages for three of the four fractions collected in the step-heating experiment are in agreement within 1σ error and represent 63.5% of the ^{39}Ar released. The plateau age of $882 \pm 189 \text{ ka}$ ($\text{MSWD} = 0.97$), calculated with the segment defined by these fractions, is the preferred age for this sample. The distribution of the data does not define a reliable isochron age. The straight line plotted in the $^{36}\text{Ar}/^{40}\text{Ar}$ versus $^{39}\text{Ar}/^{40}\text{Ar}$ correlation diagram (Figure 2e) was calculated forcing the Y intercept through $^{40}\text{Ar}/^{36}\text{Ar} = 295.5$ and is only presented for illustrative purposes.

Table 1. Summary of ^{40}Ar - ^{39}Ar Ages^a

Code No	K/Ca Total	Total Fusion Age (ka) $\pm 1\sigma$	Isochron Age (ka) $\pm 1\sigma$	$^{40}\text{Ar}/^{36}\text{Ar}_i \pm 1\sigma$	<i>N</i>	MSWD	Weighted Mean Age (ka) $\pm 1\sigma$	^{39}Ar (%)	<i>N</i>	MSWD
DG	0.443	82 \pm 106					46 \pm 123	59.34	1 of 2	—
	0.452	40 \pm 93					86 \pm 57	85.35	2 of 3	0.39
	0.441	-22 \pm 80					79 \pm 95	59.64	1 of 4	—
			166 \pm 265 ^b	292 \pm 8	9 of 9	0.67	78 \pm 56^c	59.64	4 of 9	0.11
DF	0.428	41 \pm 78								
	0.429	475 \pm 184								
	0.436	196 \pm 207								
	0.426	327 \pm 103								
	0.426	240 \pm 75					73 \pm 62	66.91	2 of 6	0.04
			81 \pm 35^b	299 \pm 1	22 of 23	1.36	109 \pm 45	80.91	2 of 4	0.6
AL2	0.525	32 \pm 68								
	0.534	298 \pm 103								
			123 \pm 94 ^b	295 \pm 13	5 of 5	4.1				
AF	0.382	334 \pm 115					318 \pm 70	100	3 of 3	0.02
	0.475	1069 \pm 114					309 \pm 49	63.37	1 of 4	—
	0.367	330 \pm 83					330 \pm 83	100	1 of 1	—
			300 \pm 83 ^b	297 \pm 5	5 of 8	0.02	315 \pm 36^c	100	5 of 8	0.02
BV	0.236	1526 \pm 261								
	0.234	3428 \pm 352					882 \pm 189	63.51	3 of 5	0.97
			1401 \pm 105	295.5 ^d	5 of 5	12.4				
AN	0.318	1334 \pm 117								
	0.334	899 \pm 77								
	0.355	1381 \pm 79								
	0.312	1213 \pm 131								
	0.298	1105 \pm 82								
			949 \pm 37^b	301 \pm 4	22 of 24	1.76				
DE	0.239	1096 \pm 148					996 \pm 168	56.66	2 of 4	0.7
	0.215	1114 \pm 135					994 \pm 174	44.19	2 of 5	<0.01
			501 \pm 527 ^b	306 \pm 9	9 of 9	0.21	995 \pm 120^c	44.19	4 of 9	0.23
DH	0.310	1381 \pm 108								
	0.286	1343 \pm 80								
			1049 \pm 81^b	303 \pm 2	11 of 11	0.24				
AO	0.240	1001 \pm 104								
	0.257	1796 \pm 162								
	0.298	989 \pm 57								
	0.302	1175 \pm 114								
	0.307	1241 \pm 72								
	0.258	989 \pm 93								
	0.324	1387 \pm 84					1137 \pm 90	57.31	2 of 6	<0.01
			1095 \pm 105^b	295 \pm 6	7 of 12	1.71	1322 \pm 100	57.31	2 of 6	<0.01
BZ	0.486	1074 \pm 85								
	0.451	1261 \pm 106								
			1414 \pm 129 ^b	285 \pm 5	4 of 4	1.5		45.66	1 of 3	—
BW	0.332	1509 \pm 69								
	0.312	1830 \pm 59					1628 \pm 56	84.77	3 of 5	1.4
			1511 \pm 206 ^b	333 \pm 34	4 of 6	5.5				

^aSite code as given in Table 2; 1σ , age uncertainty; preferred ages are indicated by bold numbers.

^bThe data from all the experiments performed with the sample were combined to calculate the isochron age

^cThe data from all the experiments performed with the sample were combined to calculate the weighted mean age

^dForced intercept ($^{40}\text{Ar}/^{36}\text{Ar}$)_i = 295.5

[19] Site AN: Three laser step-heating experiments and two step-heating experiments conducted with the temperature-controlled Ta furnace were performed with a groundmass sample, with very similar results (Figure 2f). The age spectra display a slight saddle shape, suggesting the presence of excess argon. The data of the five experiments were plotted in the $^{36}\text{Ar}/^{40}\text{Ar}$ versus $^{39}\text{Ar}/^{40}\text{Ar}$ correlation diagram. The well-defined straight line using 22 out of 24 points indicates a ($^{40}\text{Ar}/^{36}\text{Ar}$)_i = 301 \pm 4, supporting the presence of excess argon. Therefore, the preferred age is the 949 \pm 37 ka isochron age.

[20] Site DE: Two step-heating experiments were conducted with a whole rock sample using the temperature-controlled Ta furnace. The two experiments yield reproducible results. Since the sample is characterized by very low

radiogenic argon content, the data cluster is close to the *Y* axis in the $^{36}\text{Ar}/^{40}\text{Ar}$ versus $^{39}\text{Ar}/^{40}\text{Ar}$ correlation diagram (see Figure 2g). The distribution of the data does not permit to obtain a reliable isochron age. For this reason, the preferred age 995 \pm 120 ka for this sample was obtained with the weighted mean of four intermediate fractions (two of each experiment). These represent 57 and 44% of the ^{39}Ar released, respectively.

[21] Site DH: Two step-heating experiments were conducted with a groundmass sample using the temperature-controlled Ta furnace and lead to very reproducible results (Figure 2h). The age spectra are slightly saddle shaped, suggesting the presence of excess argon. The combined data of the two experiments were plotted in the $^{36}\text{Ar}/^{40}\text{Ar}$ versus $^{39}\text{Ar}/^{40}\text{Ar}$ correlation diagram, and the distribution

Table 2. Site Codes, Volcanic Province According to Figure 1 and Paleomagnetic Site Coordinates; B_C , B_{CR} , M_{RS}/M_S , Site-Averaged Hysteresis Parameters; S-300, S Ratio [Bloemendal et al., 1992]; $M_S(T)$ Type, Thermomagnetic Classification as Described in the Text (See Also Figure 2); T_C , Curie Temperatures Determined After the Method of Moskowitz [1981].

Site	Volcanic Province	Latitude (°N)	Longitude (°W)	B_C (mT)	B_{CR} (mT)	M_{RS}/M_S	S-300	$M_S(T)$ Type	T_C (°C)
DR	E-TMVB	19°07.410'	97°32.262'	22.6	38.9	0.38	0.83	A	518
AX	MG	19°28.283'	102°04.606'	13.0	34.8	0.02	0.99	A	516
AG2	VDB	19°10.620'	100°15.060'	18.8	44.8	0.29	0.99	A'	521
DV	E-TMVB	19°07.257'	97°32.245'	18.6	31.8	0.31	0.98	A'	537
AY	MG	19°29.092'	102°01.350'	9.6	15.1	0.20	1.00	E	210
BC	MG	19°24.217'	102°06.540'	13.7	29.9	0.24	0.99	A	574
EA	E-TMVB	18°55.535'	97°25.724'	12.7	32.6	0.16	0.98	A	521
DX	E-TMVB	18°56.121'	97°28.347'	17.2	68.1	0.17	0.95	C	369, 503
BB	MG	19°25.860'	102°05.260'	14.9	31.2	0.28	0.97	A	511
EG	CEB	21°11.814'	104°32.883'	7.7	22.2	0.01	0.99	A'	527
DG	VDB	19°23.490'	100°02.593'	16.2	32.3	0.20	1.00	A	535
DF	VDB	19°06.564'	99°55.896'	38.3	66.4	0.44	0.99	B	396
EJ	CEB	21°01.553'	104°23.642'	28.0	58.4	0.25	0.98	A	551
AV	CEB	21°13.060'	104°35.580'	5.8	13.0	0.10	1.00	E	291
AL2	VDB	19°09.984'	100°14.220'	19.5	35.8	0.32	0.86	G	592
CP	TEQ	20°51.960'	103°50.420'	13.2	21.4	0.27	0.99	F	250, 499
CT	TEQ	20°48.600'	103°50.700'	15.2	63.5	0.20	0.94	F	370, 580
CV	TEQ	20°47.410'	103°51.080'	13.1	32.0	0.24	0.97	F	256
BH	MG	19°25.683'	102°09.528'	11.2	27.5	0.14	0.98	A	575
DQ	E-TMVB	19°29.508'	97°08.986'	7.9	22.7	0.11	1.00	A	529
BI	MG	19°25.542'	102°26.107'	8.0	24.5	0.10	0.99	A	512
CU	TEQ	20°53.030'	103°53.960'	13.3	26.9	0.15	1.00	A'	502
CD	MG	19°23.627'	102°24.665'	14.0	37.6	0.14	0.98	A	562
AH	VDB	19°08.477'	100°10.540'	14.7	36.8	0.19	0.95	A'	526
AT	CEB	21°09.786'	104°03.900'	14.8	36.3	0.13	0.99	A'	548
AM	VDB	19°04.397'	100°15.293'	13.6	28.6	0.21	0.98	A'	562
AF	VDB	19°11.840'	100°13.208'	33.6	63.4	0.47	0.76	G	580
DT	E-TMVB	19°19.867'	97°27.214'	28.4	51.0	0.34	0.99	A	546
CF	MG	19°22.032'	102°21.953'	6.5	35.8	0.08	0.97	B	420
CY	TEQ	20°41.345'	103°55.275'	26.4	54.2	0.30	0.97	F	369, 580
BJ	MG	19°16.866'	102°23.127'	21.6	44.7	0.24	0.99	A'	532
EL	TEQ	20°49.620'	103°59.750'	7.8	14.5	0.14	1.00	A'	568
CJ	MG	19°18.600'	102°32.322'	20.5	41.2	0.25	1.00	A	528
CO	MG	19°15.443'	102°21.640'	17.9	40.0	0.17	0.99	A	485
EK	CEB	21°02.017'	104°21.617'	16.6	36.6	0.30	0.98	G	348, 534
CR	TEQ	20°51.960'	103°50.420'	14.2	39.2	0.13	0.96	A	515
AR	CEB	21°14.079'	104°47.359'	6.2	19.3	0.07	1.01	A	580
BD	MG	19°23.052'	102°05.590'	14.9	33.7	0.21	0.99	A'	573
AS	CEB	21°04.230'	104°42.700'	10.9	28.6	0.11	0.99	A	555
AQ	CEB	21°11.850'	104°47.580'	13.5	24.2	0.41	0.82	A'	538
EI	CEB	21°01.614'	104°22.750'	19.7	26.7	0.30	0.97	G	301, 568
EO	TEQ	20°53.988'	103°43.757'	6.6	16.7	0.10	1.01	A	490
EB	CEB	21°09.417'	104°42.483'	12.0	40.6	0.10	0.98	A'	525
CK	MG	19°15.760'	102°34.610'	24.0	48.1	0.24	0.99	D	314, 524
EF	CEB	21°09.192'	104°40.372'	12.0	28.1	0.13	1.00	A	517
ED	CEB	21°08.200'	104°41.817'	15.7	40.9	0.13	0.98	A	556
CW	TEQ	20°51.810'	103°58.650'	6.0	20.8	0.08	0.99	A'	533
EN	TEQ	20°53.952'	103°44.083'	7.8	14.5	0.14	0.99	A'	507
CG	MG	19°24.968	102°28.589	12.0	28.0	0.14	0.98	A'	563
CQ	TEQ	20°47.680'	103°24.430'	10.1	28.2	0.11	1.00	A	536
AZ	MG	19°26.113'	102°01.252'	18.4	30.7	0.36	0.95	A'	547
AW	MG	19°27.612'	102°03.885'	9.9	25.3	0.10	1.00	A'	555
BV	VDB	19°01.900'	100°08.912'	10.4	32.3	0.12	0.93	A'	543
CE	MG	19°15.539'	102°14.751'	16.6	39.2	0.17	0.99	A'	561
AN	VDB	19°09.037'	100°01.545'	19.9	28.8	0.42	0.99	F	368, 545
CI	MG	19°22.308'	102°29.536'	18.4	34.6	0.22	1.00	D	367, 543
DE	VDB	18°51.294'	100°07.637'	17.6	39.9	0.22	0.99	C	377, 520
DH	VDB	19°23.640'	100°01.437'	11.9	26.7	0.17	1.00	C	314, 518
CN	MG	19°28.155'	102°33.370'	6.9	18.8	0.09	1.00	A	513
AO	VDB	19°10.336'	100°07.095'	9.7	27.1	0.11	0.93	A	545
BZ	VDB	19°02.158'	100°04.678'	33.0	58.4	0.39	0.87	A'	578
BW	VDB	19°02.290'	100°10.108'	4.8	15.6	0.06	1.00	A	534
BL	MG	19°16.305'	102°04.373'	22.0	41.7	0.29	0.96	A'	577
CM	MG	19°26.592'	102°35.282'	36.3	215.1	0.30	0.65	G	507

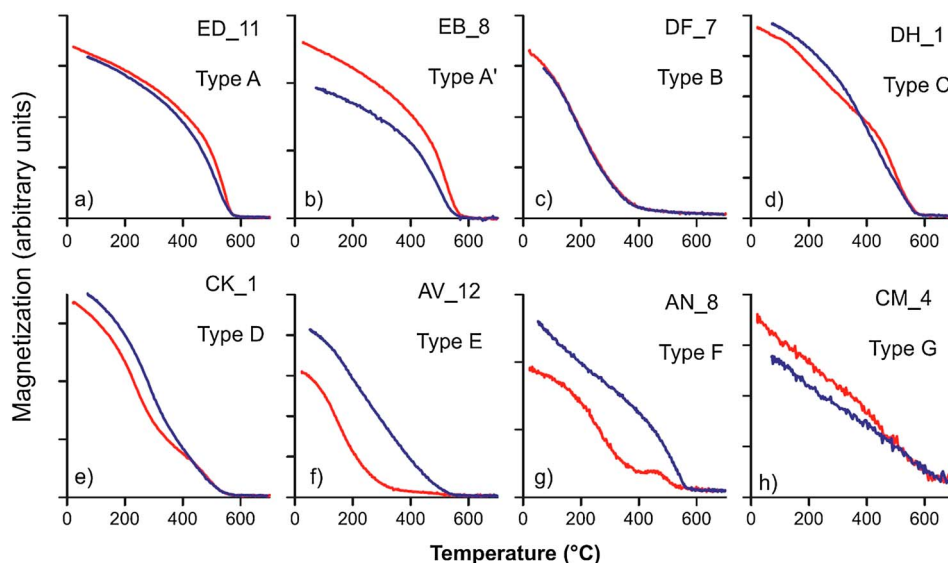


Figure 3. Different types of thermomagnetic curves obtained with a variable field translation balance (VFTB) in a field of 500 mT from room temperature to 700°C. Heating (red line) and cooling (blue line) were conducted in argon atmosphere. A correction for paramagnetic content was not necessary as magnetizations above the highest Curie temperature were small (generally between 6 and less than 2%).

of the 11 data points constrain a straight line with ($^{40}\text{Ar}/^{36}\text{Ar}$)_i = 303 ± 2 , confirming the presence of excess argon. The preferred age is the isochron age of 1049 ± 81 ka.

[22] Site AO: Six laser one-step fusion experiments plus one laser step-heating run were performed with a ground-mass sample (Figure 2i). For illustrative purposes, the six one-step experiments were plotted as a pseudo-age spectrum, where each single fusion is shown as an individual fraction. The step-heating experiment is presented at the back. All the data collected were plotted in the $^{36}\text{Ar}/^{40}\text{Ar}$ versus $^{39}\text{Ar}/^{40}\text{Ar}$ correlation diagram. The preferred age of 1095 ± 105 ka is the isochron age defined by the most radiogenic fractions of the step-heating experiment plus five out of the 6 one-step fusions. In fact, the isochron age is indistinguishable from the 1104 ± 84 ka age calculated with the weighted mean of all the one-step experiments.

[23] Site BZ: One laser step-heating and laser one-step fusion experiments were performed with a whole rock sample. The two experiments yielded similar ages; however, the analyses were conducted in very little detail (see Figure 2j). The best estimate for the age of this sample is taken from the fraction with the highest radiogenic argon yield: 1322 ± 100 ka. This age is indistinguishable within 1σ error from the 1261 ± 106 ka age obtained in the one-step fusion experiment. Due to the distribution and amount of data, the straight line defined by the four data points, in the $^{36}\text{Ar}/^{40}\text{Ar}$ versus $^{39}\text{Ar}/^{40}\text{Ar}$ correlation diagram, is not considered reliable. The preferred age for this sample is 1322 ± 100 ka.

[24] Site BW: One laser step-heating experiment and a laser one-step fusion were performed with a whole rock sample yielding similar results (Figure 2k). The bulk of the ^{39}Ar (84.77%) was released in the three middle fractions of the step-heating experiment. The weighted mean of their ages yields 1628 ± 56 ka. The data collected were plotted in the $^{36}\text{Ar}/^{40}\text{Ar}$ versus $^{39}\text{Ar}/^{40}\text{Ar}$ correlation diagram, yielding a poorly constrained isochron age of 1511 ± 206 ka. The preferred age for this sample is 1628 ± 56 ka.

6.2. Rock Magnetic Properties: Thermomagnetic Behavior

[25] Eight different types of thermomagnetic behavior (A–G) can be distinguished from the $M_S(T)$ curves (Figure 3). Type A curves show good reversibility and a single magnetic phase with a high Curie temperature between 510 and 575°C, which is indicative of Ti-poor titanomagnetite (Figure 3a). Type A' curves (Figure 3b) show similar behavior as Type A curves but with a slight decrease in magnetization on the cooling branch, probably due to the partial oxidation of such titanomagnetite to hematite during laboratory heating. Type A or A' behavior was observed in 44 out of a total of 63 samples. Type B curves (sites DF and CF) show excellent reversibility and a T_C between 320 and 420°C (Figure 3c), indicative of titanomagnetite with compositional parameter between $x \approx 0.25$ and 0.4 [O'Reilly, 1984]. Type C behavior (Figure 3d) was found in samples from three sites (DX, DH, and CN). Two Curie temperatures were observed on the heating curve, the low-temperature phase ($T_C \approx 220$ –370°C) being probably due to cation-deficient titanomagnetite, as this phase is not seen in the cooling curve, while the high-temperature phase again indicates Ti-poor titanomagnetite. Reversibility is still good, although a slight increase of M_S is observed in the cooling curve. Samples displaying two different T_C at ≈ 310 –350°C and ≈ 520 –560°C (Figure 3e) are classified as Type D samples (sites CK and CI). Curves are fairly reversible, and both T_C values are observed in the heating and cooling branches, again with a small increase of M_S in the cooling curve. This behavior is interpreted as being indicative of two different titanomagnetites with differing Ti content. Type E behavior (Figure 3f) is characterized by a single phase of titanomagnetite with a T_C between 190 and 290°C, which indicates a fairly high Ti content ($x \approx 0.6$ –0.4). Such curves (sites AY, AV, and CP) are typical for titanomagnetites where no deuteric oxidation occurred on primary cooling, but since then have undergone some low-

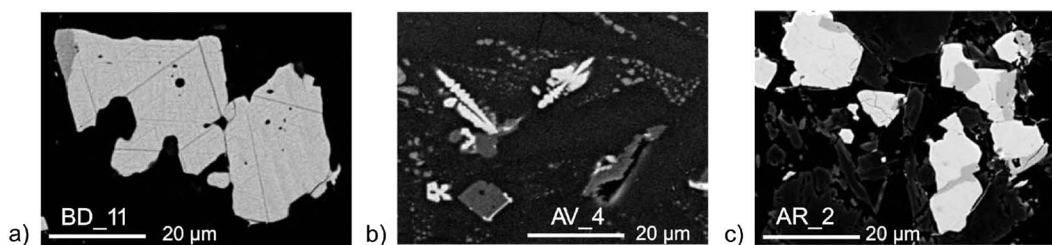


Figure 4. Zeiss DSM962 backscattered electron microscope micrographs of (a) Ti-poor titanomagnetite with ilmenite exsolution lamellae (sample BD_11 from the Michoacan-Guanajuato volcanic field; oxidation stage C3–C4), (b) Skeletal titanomagnetite grains classified as the cruciform type (sample AV_4 from the Ceboruco San-Pedro volcanic field; oxidation stage C1), (c) large unexsolved titanomagnetite grains with shrinking cracks due to low temperature oxidation/maghemitization (sample AR_2 from the Ceboruco San-Pedro volcanic field). Classifications follow *Haggerty* [1991].

temperature oxidation (maghemitization), as indicated by the irreversibility and higher M_S values seen in the cooling curve. Samples showing a titanomaghemite inversion peak at around 350 to 430° C (Figure 3g) are classified as Type F samples (sites CT, CV, CY, and AN). On continued heating above the inversion peak, titanomaghemite is transformed to a magnetic phase with a T_C of around 580°C, close to that of pure magnetite. In samples showing Type G behavior (Figure 3h), a well-defined Curie temperature is masked by a paramagnetic contribution and instrumental noise. Samples showing this rather noisy behavior (sites AL2, EK, EI, and CM) generally displayed the weakest magnetizations.

6.3. Microscopy Studies

[26] Reflected light microscopy studies revealed that samples with high Curie temperatures between 510 and 575°C and thermomagnetic behavior of type A or A' often contain intermediately exsolved titanomagnetite (oxidation stages C3–C4, after *Haggerty* [1991]) with some ilmenite lamellae (Figure 4a).

[27] Skeletal or needle-like titanomagnetite was found in lavas showing thermomagnetic Type E behavior (sites AY and AV). Here titanomagnetite appears unblemished, indicating a fast cooling of the lava before deuteric oxidation could occur (Figure 4b). This habitus is similar to the ones reported by *Urrutia-Fucugauchi et al.* [1984] from a columnar basalt from Central Mexico, or from mid-ocean ridge basalt samples reported by *Krása and Matzka* [2007]. Visual signs of maghemitization were found in samples from sites AR, BH, and CQ. Here titanomagnetite displays the typical surface cracks on the crystals, as a result from the change in volume due to diffusion of Fe^{2+} from the crystal lattice structure to the surface, where it is converted to Fe^{3+} (Figure 4c). However, the thermal stability does not seem to be greatly affected, as samples from these lavas still displayed almost reversible behavior during the thermomagnetic experiment. Samples from two sites showing thermomagnetic Type G behavior (AL2 and AF) are clearly characterized by contributions of (titano-) hematite, which likely causes the noisy behavior during the thermomagnetic experiments. These samples appeared red in color, and ore microscopy studies revealed that almost all the primary spinel minerals were altered/limonitized to rutile with goethite and lepidocrocite by low-temperature oxidation (or perhaps hydrothermal alteration, Figures 5a and 5b). However, as seen in the backscattered electron micrograph in Figure 5c,

very small titanomagnetite, often of submicron size is observed along needles of pyroxene. This titanomagnetite appears unblemished and probably remained unaffected by the oxygen fugacity. In samples from site AQ, characterized by (titano-) hematite, large titanomagnetite grains showed signs of replacement stage oxidation (C6) as indicated by the graphical/myrmecitic intergrowth of pseudobrookite (Figures 5d and 5e).

6.4. Rock Magnetic Properties: Hysteresis Properties

[28] Figure 6 shows six examples of hysteresis data with corresponding IRM acquisition curves, and Figure 7 shows the Day plot, generated from the hysteresis parameters tabulated in Table 2. In Figures 6a–6c, hysteresis loops are shown that are characteristic for the majority of samples investigated in this study. No wasp-waisted behavior is observed near the origin of these loops, which indicates restricted coercivities [*Tauxe et al.*, 1996], and IRM curves are fully saturated at fields of 100–300 mT. Samples from site CV (Figure 6d) are characterized by a bimodal distribution of coercivities (as seen in the IRM acquisition rate), and the hysteresis loop is wasp waisted. As these samples are characterized by low Curie temperatures, it is likely that aside from a titanomagnetite with high Ti content, some additional magnetite is present. Thus, this behavior probably relates to two fractions of titanomagnetite and magnetite. Samples characterized by contributions of (titano-) hematite had clearly wasp-waisted loops, and their IRM acquisition curves are not saturated at IRM peak fields of 2 T (Figures 6e and 6f). As hysteresis measurements were carried out to a maximum field of 1 T, M_S is underestimated, and consequently, these samples plot away from the mixing lines, more toward the right side of the Day plot (Figure 7), particularly obvious for samples from site CM. The majority of samples plot within the pseudosingle domain range along the theoretical linear mixing curves of *Dunlop* [2002].

[29] Due to the information gained from rock magnetic analyses, we interpret low Ti titanomagnetite as the remanence carrier in the majority of samples from this study. Samples are considered to be mixtures of single domain (and/or pseudosingle domain) and multidomain particles. Small contributions of (titano-) maghemite are probably present in samples from nine sites (AY, AV, CP, CT, CV, CY, and AN) as indicated by the thermomagnetic behavior (Types E and F behavior, Figure 3) and ore microscopy

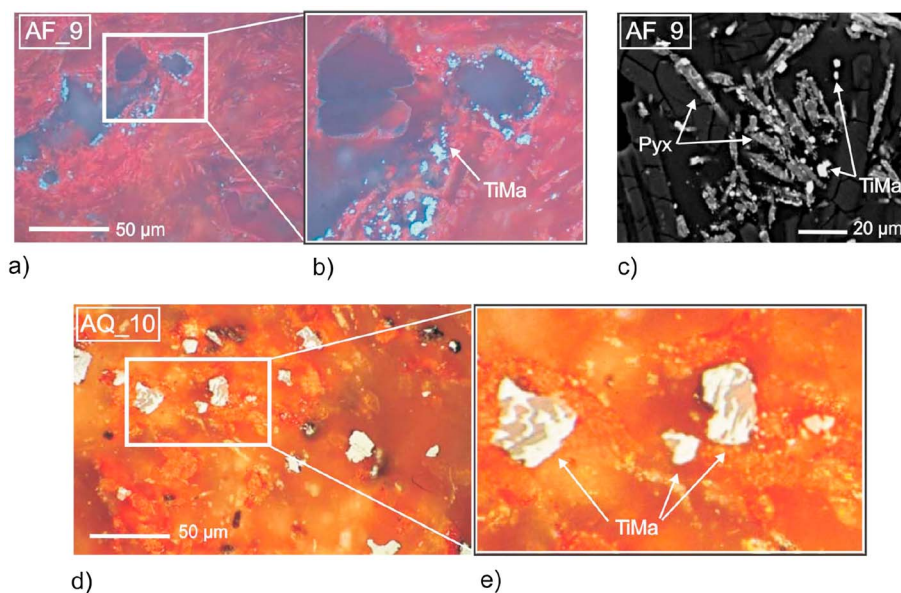


Figure 5. Examples of reflected-light microscopy; (a–c) highly oxidized lava (sample AF_9 from the Valle de Bravo volcanic field), dominated by (titano-) hematite, which appears red in color; (b, inset) small titanomagnetites (TiMa) unaffected by alteration, which appear grey in color; (c) backscattered electron microscope micrograph from the same sample, showing small unblemished titanomagnetites (in bright color) along needles of pyroxene (Pyx, grey in color); (d and e) sample AQ_10 from the Ceboruco San-Pedro volcanic field, dominated by (titano-) hematite with large titanomagnetite grains showing signs of replacement stage oxidation (oxidation stage C7).

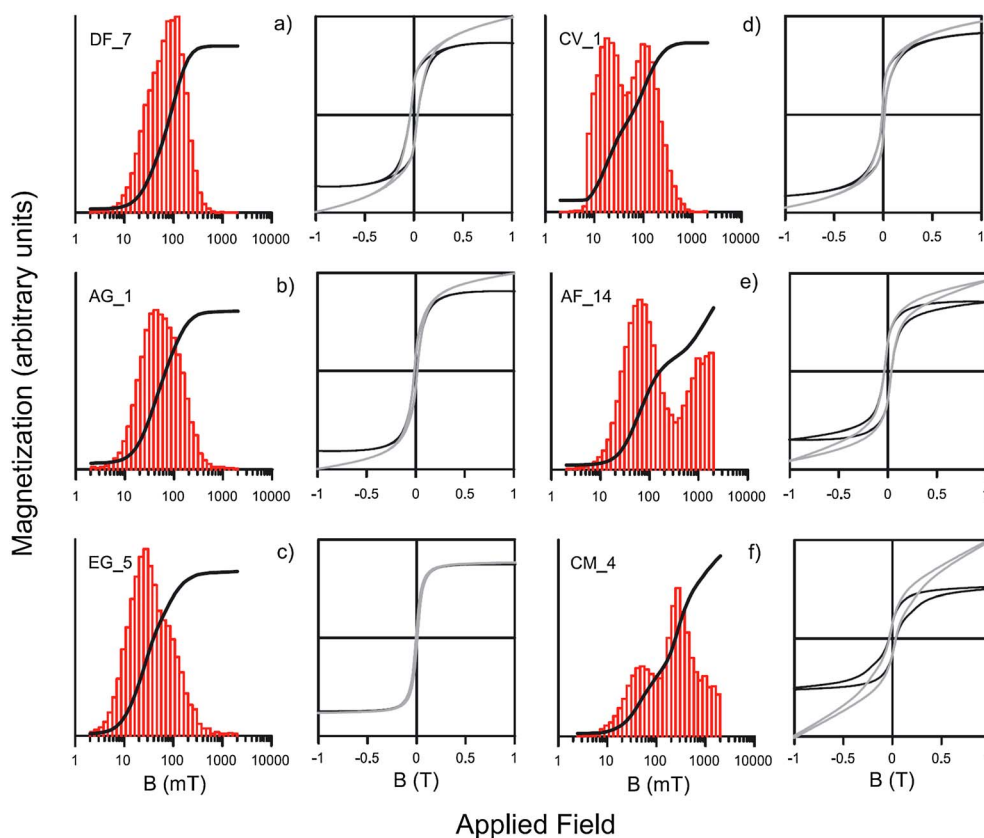


Figure 6. Examples of hysteresis loops, black line (grey line) corrected (uncorrected) for paramagnetic content and corresponding acquisition curves (solid line) and acquisition rates per field step (red bars) of the isothermal remanent magnetization (IRM).

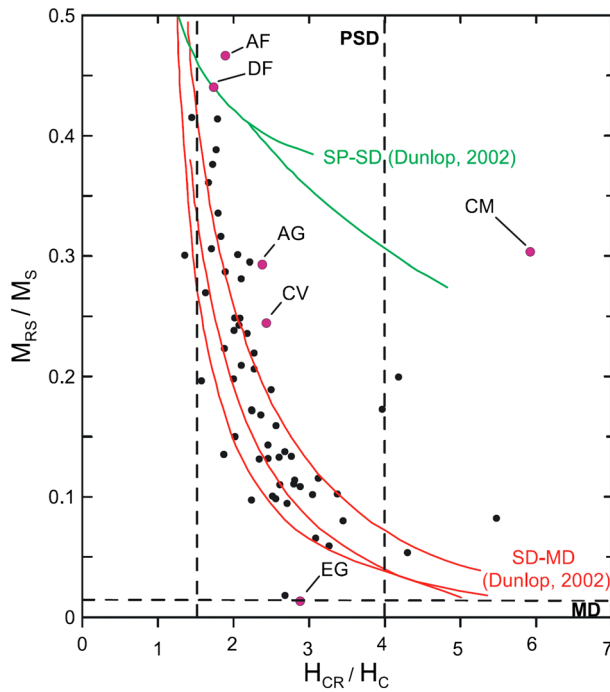


Figure 7. Plot of bulk magnetic domain states [Day *et al.*, 1977] for site-averaged hysteresis parameters of the 63 lavas investigated in this study. Theoretical mixing curves of Dunlop [2002] are shown for reference; single domain-multidomain (red lines) and super paramagnetic-single domain (green lines); data from samples shown in Figure 5 (magenta).

(AR, BH, and CQ), while samples from four sites (AL2, AF, AQ, and CM) additionally contain (titano-) hematite.

6.5. Paleomagnetic Directions

[30] A characteristic remanent magnetization (ChRM) was successfully isolated by either AF or thermal demagnetization for most samples and determined using principal component analysis [Kirschvink, 1980], following the quality criteria of Tauxe *et al.* [2000], by using at least five vector endpoints and a maximum angular deviation of less than 5° . Secondary viscous remanent magnetizations (VRMs) that were easily removed by AF fields of 10–15 mT or thermal demagnetization to 200°C (Figure 8a) were common. Occasionally, the vector sum of the VRM component was larger than from the ChRM (Figure 8b). In some cases, we observed that small quantities of NRM (5–15%) persisted after peak AF demagnetization fields of 100–125 mT. However, as these samples generally displayed a linear decay of remanence toward the origin of the vector endpoint diagrams, and sister samples subjected to thermal demagnetization displayed similar directional behavior, we are confident that the ChRM was correctly identified. In some samples subjected to thermal demagnetization, most of the NRM was removed between 450° and 550°C (Figure 8c). For samples containing (titano-) hematite, AF peak fields of 100–125 mT were not sufficient to fully demagnetize the NRM, leaving as much as 30–50% of the NRM intact (Figure 8d). This demagnetization behavior correlates with samples showing nonsaturated hysteresis loops. In such cases, a combined demagnetization approach of AF and

thermal demagnetization was used (Figure 8e). Samples with reversed magnetizations often showed a normal polarity viscous overprint, oriented antiparallel to the ChRM of reversed polarity, resulting from the post-reversal field (Figure 8f). Occasionally, significant secondary components were observed, which are likely due to a lightning-induced IRM (Figure 8g). This was supported by anomalously high NRM intensities, higher than those obtained from unaffected samples of the same flow. Such samples were rejected from further analysis.

[31] Mean paleomagnetic directions (Table 3 and Figure 9) were calculated from at least three, on average 10, samples applying Fisher statistics [Fisher, 1953]. Fifty-one mean vectors have α_{95} values between 2° and 9° with an average of 6.1° , while eight sites (BH, CU, EO, CK, AZ, CI, CG, and DE) have α_{95} values $>10^\circ$. Flow AM was affected by lightning to such a degree that it was not possible to determine reliable ChRM directions. Four sites (DG, AS, EI, and EF) had dispersed paleomagnetic directions and were rejected. Virtual geomagnetic poles (VGPs) were calculated from the site mean directions and are shown in Figures 10a and 10b for normal and reverse polarities, respectively.

7. Discussion

7.1. Paleosecular Variation

[32] To avoid using tectonically affected sites in the calculation of PSV, we restricted the analysis to lavas of Pleistocene age (younger than 1.8 Ma) because tectonic rotations may be significant in the TMVB for rocks exceeding that time range [Ruiz-Martinez *et al.*, 2000]. Figure 10 shows a polar plot of virtual geomagnetic pole positions for normal and reversed polarity sites with Brunhes-aged lavas indicated by red circles and Matuyama-aged lavas by green diamonds. This indicates that two Brunhes-aged lavas have reversed polarity and seven sites of Matuyama age have normal polarity magnetizations. A possible relationship of these lavas with regard to geomagnetic excursions is discussed below.

[33] Paleosecular variation S_b is estimated from the scatter of VGPs, determined by the root mean square angular deviation of VGPs by

$$S_b = \sqrt{\frac{1}{N-1} \sum_{i=1}^N \delta_i^2 - \left(\frac{S_w^2}{\bar{n}}\right)} \quad (1)$$

where δ_i is the angular distance (AD) of the VGP for the i th site from the mean VGP, N is the number of sites used in the calculation, and S_b is the geomagnetic signal remaining after correcting for within-site dispersion S_w and using the mean number \bar{n} of samples per site [Johnson *et al.*, 2008].

[34] The global database of PSV, based on a compilation of 0–5 Ma lavas (Model G) [McFadden *et al.*, 1988, 1991], predicts an increase of S with latitude. For Model G, the predicted value for the latitude of Mexico of 20° is $S = 13.4_{12.9}^{14.0}$ (upper and lower confidence limits, respectively). A similar latitudinal trend is predicted by Model TK03 [Tauxe and Kent, 2004], which is based on a time-averaged field specified by GAD and 10,000 simulations at latitude increments of 5° using the McElhinny and McFadden [1997] high-quality data compilation (DMAG 4 criteria). The TK03

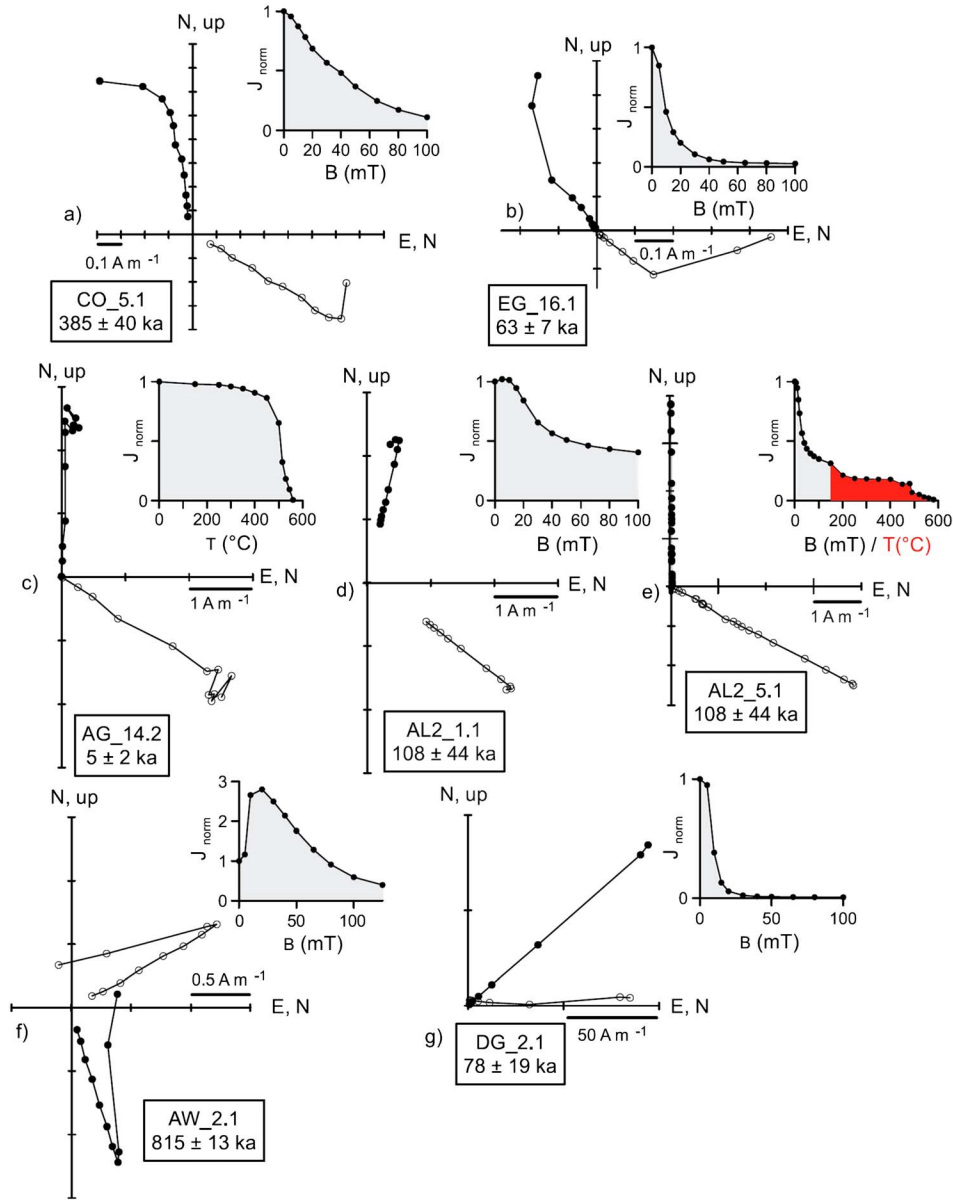


Figure 8. Orthogonal vector endpoint diagrams of representative demagnetization data, solid circles (open circles) are projections into the horizontal (vertical, defined by the horizontal component of the direction vector) plane and normalized intensity decay curves.

Model predicts $S = 12.9^{13.0}_{12.7}$. Recently, *Johnson et al.* [2008] presented a new model for the 0–5 Ma time-averaged field, which we refer to as TAF-J. The TAF-J model is based on high-quality paleomagnetic directional data from over 2000 volcanic sites with sufficient spatial and temporal sampling, spanning latitudes from $78^{\circ}S$ to $53^{\circ}N$. It indicates a different latitudinal structure of PSV for the Brunhes and Matuyama Chrons, with less latitudinal variation of PSV for normal polarity Brunhes data ($S=16$) and generally higher dispersion and some latitude dependence for reverse polarity Matuyama data ($S = 13.2^{15.8}_{10.7}$). The dispersion predicted by the TAF-J model based on normal polarity Brunhes data ($S = 11.2^{12.2}_{10.1}$, for latitude 20°) is lower than the one predicted by Model G, but it has to be noted that this value is largely based on data

from Hawaii [*Lawrence et al.*, 2006], which was found to show large negative mean inclination anomalies and small dispersion. For the 0–5 Ma combined normal and reverse polarity data, *Johnson et al.* [2008] quoted a dispersion of $S = 14.5^{15.2}_{13.8}$. [35] For estimating the PSV, reversed polarity mean directions were inverted to normal polarity, thus assuming symmetry in normal and reverse polarity fields. Choosing the correct cutoff angle (λ_{cut}) to separate normal PSV from an intermediate/transitional geomagnetic regime is still a matter of debate. Some previous paleomagnetic studies from Mexico [*Petronille et al.*, 2005, *Ceja et al.*, 2006, *Conte et al.*, 2006] combined two parameters: (1) a VGP latitude lower than 60° and (2) an angular distance from the mean direction exceeding 30° . We chose a cutoff angle of 40° from the north geographic pole, which corresponds

Table 3. Flow-Mean Paleomagnetic Data^a

Site	Age (ka)	Ref.	n/N	k	α_{95} (deg)	Dec (°E)	Inc (deg)	P lat (°N)	P long (°E)	dp (deg)	dm (deg)	Pol.
DR	0 ± 20	8	9/10	233.7	3.4	9.6	27.8	79.8	16.4	2.0	3.7	N
AX	2 ± 10	4	13/16	22.9	8.8	334.9	37.1	66.4	175.3	6.1	10.3	N
AG2	5 ± 2	5	5/5	302.4	4.4	2.4	17.7	79.9	66.5	2.4	4.6	N
DV	16.8 ± 0.75	2	8/9	230.8	3.4	11.5	25.5	77.6	18.1	2.0	3.7	N
AY	23 ± 31	4	10/16	43.2	7.4	5.4	33.2	84.7	2.1	4.8	8.4	N
BC	26 ± 58	4	16/16	20.1	8.4	18.2	33.9	72.8	347.7	5.5	9.6	N
EA	31.7 ± 1.1	2	9/10	60.2	6.7	355.2	36.0	85.4	186.3	4.5	7.8	N
DX	46 ± 0.07	2	15/15	55.2	5.2	1.5	31.4	87.6	46.3	3.3	5.8	N
BB	47 ± 45	4	12/14	23.6	9.1	1.5	31.8	87.4	44.8	5.7	10.2	N
EG	63 ± 7	7	16/16	52.2	5.3	330.7	51.0	61.9	193.5	4.8	7.2	N
DG	78 ± 56	1	0/10	n.a.	n.a.	n.a.	n.a.	n.a.	n.a.	n.a.	n.a.	n.a.
DF	81 ± 35	1	9/10	67.6	6.3	12.0	31.8	78.4	357.5	7.1	7.1	N
EJ	85 ± 19	7	14/14	83.9	4.4	350.4	49.2	77.5	213.3	3.9	5.8	N
AV	108 ± 22	7	10/14	36.0	8.2	12.4	24.5	75.5	18.7	4.7	8.8	N
AL2	109 ± 45	1	9/10	109.2	4.9	6.6	33.2	83.7	358.2	3.2	5.6	N
CP	178 ± 8	6	7/13	71.8	7.2	333.6	23.2	63.3	151.2	4.1	7.7	N
CT	191 ± 13	6	7/8	48.5	8.8	359.2	28.8	84.6	78.2	5.3	9.7	N
CV	196 ± 8	6	8/10	42.1	8.6	358.8	24.8	82.1	84.7	5.0	9.2	N
BH	230 ± 68	4	14/14	10.0	13.3	2.8	29.3	85.4	42.0	8.1	14.7	N
DQ	240 ± 50	10	10/12	76.8	5.5	357.7	32.0	86.9	128.8	3.5	6.2	N
BI	256 ± 9	3	12/13	20.1	9.9	19.5	34.8	71.6	345.1	6.6	11.4	N
CU	261 ± 11	6	9/11	21.8	11.3	334.5	55.7	63.0	206.2	11.6	16.2	N
CD	269 ± 11	3	12/13	141.9	3.7	1.9	24.3	83.1	62.0	2.1	4.0	N
AH	282 ± 5	5	6/7	56.8	9.0	4.9	29.2	84.1	26.0	9.9	5.5	N
AT	283 ± 5	7	10/12	105.1	5.0	351.3	34.3	81.5	150.9	3.3	5.7	N
AM	290 ± 12	5	0/12	n.a.	n.a.	n.a.	n.a.	n.a.	n.a.	n.a.	n.a.	n.a.
AF	315 ± 36	1	17/21	39.9	5.7	358	39.9	84.9	102.1	3.4	6.2	N
DT	330 ± 80	9	16/16	53.8	5.1	9.0	47.6	77.5	302	4.3	6.6	N
CF	339 ± 11	3	8/9	74.0	6.5	7.3	34.3	83.1	350.8	4.3	7.4	N
CY	354 ± 15	6	11/12	60.9	5.9	323.6	37.6	56.1	173.4	4.1	6.9	N
BJ	360 ± 30	4	15/16	147.2	3.2	6.7	33.0	83.5	358	2.1	3.6	N
EL	362 ± 13	6	15/16	56.4	5.1	358	35.8	87.9	138.4	3.4	5.9	N
CJ	373 ± 30	3	11/12	37.1	7.6	8.0	33.6	82.4	353.2	4.9	8.7	N
CO	385 ± 20	3	12/12	166.1	3.4	357	33.3	87	144.4	2.2	3.9	N
EK	403 ± 15	7	7/8	115.4	5.6	4.7	49.7	79.6	278.7	5.0	7.5	N
CR	416 ± 3	6	14/16	78.4	4.5	0.3	26.7	83.3	73.7	2.7	4.9	N
AR	425 ± 130	7	12/15	34.4	7.5	13.7	23.5	74.1	17.4	4.3	8.0	N
BD	429 ± 32	3	14/15	32.2	6.9	14.2	35.9	76.6	343.3	4.3	7.4	N
AS	512 ± 34	7	0/16	n.a.	n.a.	n.a.	n.a.	n.a.	n.a.	n.a.	n.a.	n.a.
AQ	520 ± 25	7	16/16	182.6	2.7	15.0	15.0	70.2	26.1	1.4	2.8	N
EI	521 ± 15	7	0/16	n.a.	n.a.	n.a.	n.a.	n.a.	n.a.	n.a.	n.a.	n.a.
EO	592 ± 20	6	11/13	17.2	11.3	172.3	-21.1	-77.6	294.0	6.3	11.9	R
EB	601 ± 6	7	9/10	39.0	8.3	7.8	39.8	82.6	332.5	6.0	10.0	N
CK	612 ± 20	3	6/6	14.0	18.6	12.8	12.8	68.3	21.2	9.7	19.0	N
EF ^b	614 ± 16	7	7/10	15.5	15.8	355.1	9.9	73.2	92.5	8.1	15.9	N
ED	623 ± 91	7	11/15	30.0	8.5	358.6	17.3	77.6	81.8	4.6	8.8	N
CW	632 ± 8	6	10/12	122.3	4.4	5.2	26.9	81.7	38.4	2.6	4.8	N
EN	671 ± 12	6	10/11	52.3	6.7	210.3	-33.0	-61.3	166.8	4.3	7.6	R
CG	673 ± 10	3	9/11	20.0	11.8	231.3	-43.1	-42.9	150.9	9.1	14.6	R
CQ	691 ± 26	6	10/10	87.0	5.2	1.7	27.5	83.6	61.4	3.1	5.7	N

Table 3. (continued)

Site	Age (ka)	Ref.	<i>n</i> / <i>N</i>	<i>k</i>	α_{95} (deg)	Dec (°E)	Inc (deg)	<i>P</i> lat (°N)	<i>P</i> long (°E)	<i>dp</i> (deg)	<i>dm</i> (deg)	Pol.
AZ	730 ± 113	4	10/13	20.7	10.9	9.8	45.3	78.4	306.9	8.8	13.8	N
AW	815 ± 13	4	14/16	50.5	5.6	164.8	-24.1	-73.4	321.7	3.1	5.9	R
BV	881 ± 189	1	10/11	184.6	3.6	357.3	11.8	76.7	91.6	3.7	1.9	N
CE	909 ± 11	4	13/14	42.2	6.5	186.9	-32.0	-83.2	182.9	4.1	7.3	R
AN	949 ± 37	1	10/12	34.6	8.3	348.8	27.8	77.6	210.5	8.7	4.7	N
CI	957 ± 157	4	13/13	16.1	10.6	15.3	51.9	71	300.6	9.9	14.5	N
DE	995 ± 120	1	6/10	19.6	15.5	352.9	15.3	77	112.8	8.2	15.9	N
DH	1049 ± 81	1	3/3	540.6	5.3	185.4	-24.8	-81.8	220.1	3.1	5.7	R
CN	1075 ± 34	3	10/11	51.5	6.8	22.6	25.4	67.5	359.8	3.9	7.3	N
AO	1095 ± 105	1	8/8	82.0	6.2	3.8	-18.3	61.6	286.2	6.2	3.2	N/I
BZ	1322 ± 100	1	14/16	74.2	4.6	194.1	-19.3	-73.6	201.7	2.5	4.8	R
BW	1628 ± 56	1	11/12	25.5	9.2	6.8	36.2	83.5	339.3	10.7	6.2	N
BL	3528 ± 64	4	16/16	177.9	2.8	334.8	1.0	59	133.6	1.4	2.8	N/I
CM	6461 ± 33	4	9/10	45.2	7.7	0.4	46.2	81.9	259.9	6.3	9.9	N

^aSite EF. Age with 1σ error; Ref., reference for age determination: (1) this work, (2) *Schaaf and Ramirez-Luna* [2008], (3) *Owby et al.* [2007], (4) *Owby et al.* [2011], (5) *Blatter et al.* [2001], (6) *Lewis-Kenedi et al.* [2005], (7) *Frey et al.* [2004], (8) *Ori and Carrasco-Niñez* [2009], (9) *Carrasco-Niñez et al.* [2007], and (10) *Carrasco-Niñez et al.* [2010]; most of the Ar/Ar studies reported their ages relative to Fish Canyon Tuff biotite of 27.99 ± 0.04 Ma (apart from Blatter et al, who used Fish Canyon Tuff sanidine of 28.02 Ma). In this study, monitors used were sanidine TCR of 28.34 ± 0.28 Ma, biotite HD-B1 of 24.18 ± 0.09 Ma, and internal standard biotite CATAV 7-4 of 89.13 ± 0.35 Ma, see text for details. *n*, number of specimens used for the calculation of the mean direction; *N*, number of measured samples; *k* and α_{95} , precision parameter and radius of 95% confidence cone of Fisher statistics [Fisher, 1953], respectively; Dec, declination; Inc, inclination; *P* lat/*P* long, latitude/longitude of the corresponding virtual geomagnetic pole; *dp* and *dm*, axes of the 95% confidence error oval of virtual geomagnetic poles; Pol., magnetic polarity (N, normal polarity; R, reversed polarity; I, intermediate direction); n.a., not available/discarded data.

^bAffected by lightning strikes and the site mean direction may still be affected to some degree by secondary components; this site is only considered for magnetostratigraphy interpretation and not used for PSV analysis.

Table 4. Summary Statistics of Paleosecular Variation Estimates Obtained From Data of Lava Flows Younger Than 1600 ka and for Data From Lava Flows Dating of Brunhes Chron and Matuyama Chron Separately^a

Data Set	Selection Criteria	N_o	N	λ_{cut}	AD max	S_{tot}	S_l	S	S_u
All data	Fixed cutoff of 40°	57	56	40.0	36.6	14.5	11.3	14.0	16.7
	Vandamme	57	49	22.2	19.7	10.2	7.8	9.6	11.1
	$N > 4, k > 50$								
	Fixed cutoff of 40°	31	31	40.0	35.6	15.5	11.0	15.3	18.8
Brunhes data	Vandamme	31	26	22.1	18.7	10.0	7.5	9.7	11.7
	Fixed cutoff of 40°	46	45	40.0	36.3	14.1	10.3	13.6	16.7
	Vandamme	46	39	19.7	18.1	9.0	6.8	8.3	9.8
	$N > 4, k > 50$								
Matuyama data	Fixed cutoff of 40°	26	26	40.0	34.7	14.2	9.3	13.9	18.1
	Vandamme	26	23	19.2	16.4	8.3	5.5	7.9	9.7
	Fixed cutoff of 40°	11	11	40.0	28.6	16.5	11.0	16.0	20.1

^aA fixed cutoff of 40° is applied, and in a second calculation, cutoff values are calculated after the method of *Vandamme* [1994]. N_o/N , number of sites available/used in the calculation of the scatter of virtual geomagnetic poles; λ_{cut} , cutoff angle used in the calculation; AD max, maximum angular distance from the North Pole of VGP included in the calculation; S_l , total scatter of VGPs; S_u , within-site dispersion; S_b , between-site dispersion of VGPs; S_u and S_l , upper and lower confidence limits of S_b , calculated after the method of *Cox* [1969].

to a VGP latitude of 50°. Additionally, VGP cutoff values were calculated using the method of *Vandamme* [1994], in which the cutoff value is a function of the VGP scatter, calculated from Model G [*McFadden et al.*, 1988, 1991] according to

$$\lambda_{cut} = (1.8S + 5)^\circ \quad (2)$$

[36] As the S values did not converge when removing low-latitude VGPs, we decided to select from the iterative process an intermediate S of 10° for Brunhes and combined Brunhes-Matuyama data, and 11° for Matuyama data. Both cutoff approaches (40° fixed cutoff and Vandamme cutoff) were applied, and results are listed in Table 4.

[37] Using a constant cutoff of 40°, we obtain dispersion values, which are consistent within the error range with Models G, TK03, and TAF-J. For combined Brunhes and Matuyama data, we obtain $S_b = 14.2$, and slightly higher values $S_b = 15.4$ when restricting the analysis to high-quality data ($n > 4, k > 50$) only. Treating Brunhes data separately gives a slightly lower dispersion of $S_b = 13.8$ for all data and $S_b = 14.3$ for high-quality data. Matuyama data indicate some higher dispersion of $S_b = 16.2$, although only 11 VGPs have been used in the calculation. The average number of samples per site was for all analyzed data sets $\bar{n} > 10$.

[38] Significantly lower dispersion values are obtained when applying the cutoff criteria of *Vandamme* [1994] given above, which removed eight VGPs from the Brunhes-Matuyama data set and reduced the dispersion significantly to $S_b = 10.9$. For the Matuyama data set, this approach worked better, eliminating only one VGP, and this leads to an $S_b = 14.9$ which is comparable to the dispersion for the Brunhes data using the 40° cutoff angle or using high-quality data only. The Vandamme approach applied to the Brunhes data removed many VGPs with latitudes $> 60^\circ$, which we regard to be still within the range of normal PSV, and in consequence, we favor the fixed cutoff approach. In summary, PSV estimates from this study indicate “normal” values of PSV for Mexico, best described by latitude-dependent models (Model G, TK03, and TAF-J). This is in agreement with previously published PSV estimates from the TMVB covering a similar time window [e.g., *Mejia et al.*, 2005].

7.2. Correlation to the Geomagnetic Instability Timescale

[39] Flow-mean VGP latitudes, declinations, and inclinations are depicted in Figure 10 against their age position in the geomagnetic polarity timescale supplemented with excursions reported in the literature. Most ages of geomagnetic excursions within the Brunhes Chron are adopted from the geomagnetic instability timescale of *Singer et al.* [2002, 2008a, 2008b] and from sedimentary data from numerous ODP (Ocean Drilling Project) paleomagnetic studies summarized by *Lund et al.* [2006]. Excursions within the Matuyama are mainly adopted from *Singer and Brown* [2002] and sedimentary data from ODP sites 983/984, Iceland Basin [*Channell et al.*, 2002]. The latter is most likely the best dated

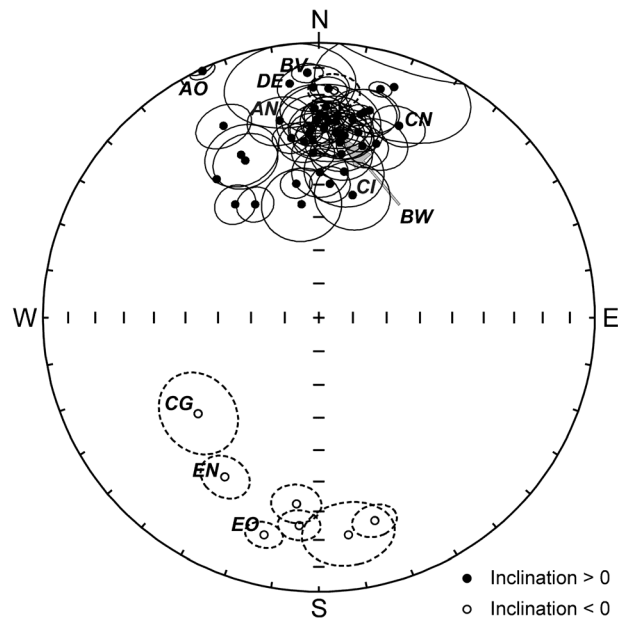


Figure 9. Equal area projection of all mean characteristic remanent magnetization directions with 95% confidence circles. Black dots (open circles) are projections on the lower (upper) hemisphere. Directions of excursions or events are labeled with the corresponding site codes (see Table 2).

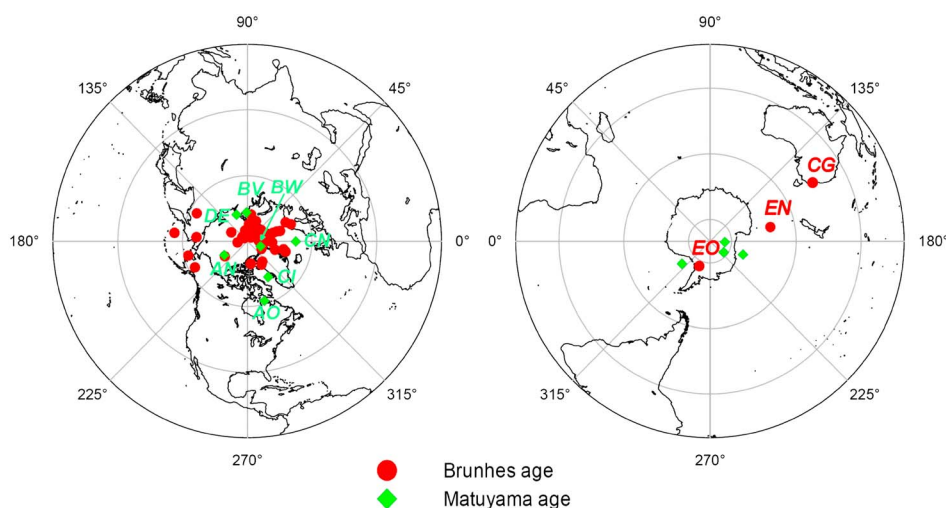


Figure 10. Polar projection of virtual geomagnetic poles from sites dating of Brunhes Chron (red dots) and Matuyama Chron (green diamonds). (a) Sites with normal polarity and (b) sites with reversed polarity. VGPs corresponding to excursions or events are labeled with their corresponding site codes (see Table 2).

(by a continuous stable oxygen isotope astrochronologic age model) and one of the most highly resolved marine sediment sequences covering the lower Brunhes and most of the Matuyama Chron. In the following, we discuss paleomagnetic data which according to our studies and/or those of *Petronille et al.* [2005] and *Ceja et al.* [2006] may be associated with geomagnetic excursions and events. Representative demagnetization data of sites that are discussed are shown in Figures 11 and 12 to demonstrate that the ChRM has been reliably determined, even in cases where relatively strong instable components were present, like in sample EN_4.1. Such components were removed in AF amplitudes < 50 mT or by thermal demagnetization below 400°C . Below, we use the term *fully reversed* when the VGP latitude is less than -45° for Brunhes data and larger than 45° for Matuyama data.

[40] 1. Site CY (354 ± 15 ka) [Lewis-Kenedi et al., 2005] has a normal polarity mean direction of $D=323.6^{\circ}$, $I=37.6^{\circ}$, $\alpha_{95}=5.9^{\circ}$, $n/N=11/13$ (n =number of samples used in the calculation, N =number of treated samples), $P_{\text{lat}}=56.1^{\circ}$. *Ceja et al.* [2006] obtained a rather poorly defined result based only on three accepted, but four rejected, samples ($D=290.5^{\circ}$, $I=14.5^{\circ}$, $\alpha_{95}=14.5^{\circ}$, $n/N=3/7$, $P_{\text{lat}}=24.9^{\circ}$; site TM10 in their publication) and interpreted the direction as intermediate. Using the quoted GPS coordinates, which are identical to those given by *Lewis-Kenedi et al.* [2005] for their $^{40}\text{Ar}/^{39}\text{Ar}$ dating sample but where the block lava exposure was rather poor, we were unable to identify their sampling locality. *Ceja et al.* [2006] interpreted the intermediate direction as new volcanic evidence for the Levantine event, first proposed by *Ryan* [1972], which is one of the rather poorly defined events in the Brunhes and which occurred at about 360 ka [Singer et al., 2002]. We sampled about 350 m to the west an outcrop along the flow surface, as suggested by field observation and Google Earth images. Sampling covered an interval of ~ 15 m, where five different blocks could be distinguished. Our result (Figure 12a) is based on more drill cores that produced coherent directions, and while it is significantly different from the result published by *Ceja et al.* [2006], it is of much better

quality. Assuming a VGP cutoff angle of 40° , it lies also still within the range of usual PSV. Considering the generally rather poor outcrop exposures at this site and the incoherent paleomagnetic results, future sampling of a better outcrop of this flow, for both paleomagnetic and geochronology studies, is required to accept this lava flow as being excursive, if at all. Based on all available data, this does not seem to be the case.

[41] 2. Site TM9 in the same study of *Ceja et al.* [2006], dated at 362 ± 13 ka [Lewis-Kenedi et al., 2005], was also linked to the Levantine event. Here they obtained a direction of $D=23.3^{\circ}$, $I=5.8^{\circ}$, $\alpha_{95}=6.2^{\circ}$, $n/N=9/12$, $P_{\text{lat}}=61.3^{\circ}$, which was again interpreted as intermediate. Again, the blocky lava exposure was rather poor, with many moved blocks, and no boreholes were spotted at the cited GPS coordinates. Our site EL corresponds to that same dated flow but is situated about 250 m south of the geochronology location. We distributed our samples over a large interval (>30 m) and sampled 10 independent blocks interpreted as original in situ cooling structures. A well-defined normal polarity magnetization of $D=358^{\circ}$, $I=35.8^{\circ}$, $\alpha_{95}=5.1^{\circ}$, $n=15/16$, $P_{\text{lat}}=87.9^{\circ}$ was obtained (Figure 12b). We propose therefore that our fully normal paleodirection supercedes TM9 of *Ceja et al.* [2006].

[42] 3. Flow EO (592 ± 20 ka [Lewis-Kenedi et al., 2005]; Figure 13a) has a reversed polarity magnetization of $D=173.3^{\circ}$, $I=-21.1^{\circ}$, $\alpha_{95}=11.3^{\circ}$, $n=11/14$, $P_{\text{lat}}=-77.6^{\circ}$. According to its age, this flow could have erupted during the Big Lost excursion, initially constrained by K-Ar dating of a transitionally magnetized lava flow in Idaho to 565 ± 28 ka by *Champion et al.* [1988]. The best estimated age for the Big Lost excursion is a weighted mean age of 579 ± 6 ka [Singer, 2007], based on high-quality $^{40}\text{Ar}/^{39}\text{Ar}$ age data obtained from transitionally magnetized lava sequences on La Palma (Canary Islands) dated by *Singer et al.* [2002] and on Tahiti [Hoffman and Singer, 2004]. Further volcanic evidence for this excursion comes from a group of three excursive flows (two of them with low paleo-intensities) from the West Eifel, Germany, initially studied by *Böhnel et al.* [1987], *Schnepp* [1994], and

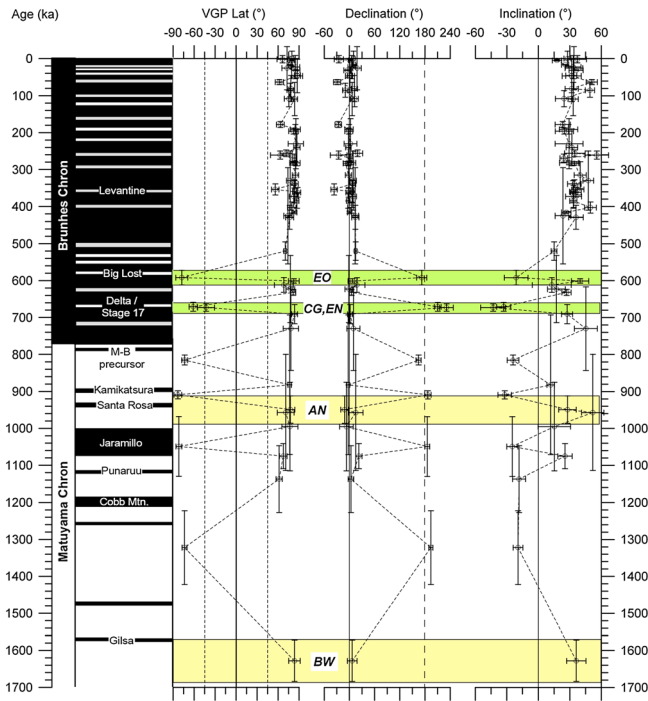


Figure 11. Paleolatitudes of the virtual geomagnetic poles (cutoff angle of 40° is indicated by the stippled line), flow-mean magnetic declinations and inclinations (geocentric axial dipole inclination indicated by the stippled line) of lavas investigated in this study with a tentative correlation to the geomagnetic polarity timescale modified for geomagnetic excursions of the last 2 Ma compiled from *Langereis et al.* [1997], *Nowaczyk and Frederichs* [1999], *Singer et al.* [2002, *Singer, 2007, Singer et al., 2008a, 2008b*], *Nowaczyk and Knies* [2000], *Channell et al.* [2002], and *Lund et al.* [2006]. Excursions highlighted in white are well-documented excursions with acceptable age control. Excursions highlighted in grey indicate excursions with restricted age control, which require further ratification. Sites that are associated with Brunhes (Matuyama) Chron excursions are highlighted with green (yellow) bands and are indicated by red stars.

Schnepf and Hradetzky [1994] and dated by *Singer et al.* [2008b] at 578 ± 8 ka. Furthermore, relative paleo-intensity minima of global extent have been found in numerous other studies with ages between 590 and 610 ka [e.g., *Lund et al., 1998; Guyodo and Valet, 1999; Channell et al., 2004*], which are most likely linked to the Big Lost excursion. We note that *Ceja et al.* [2006] also sampled this flow at their locality TL-9 about 200 m south of EO but were not successful in obtaining a mean direction. This was also the site reported for the geochronology sampling.

[43] Further evidence for the Big Lost excursion, recorded in lavas from Mexico, comes from the study of *Petronille et al.* [2005], who found two lava flows with fully reversed polarity magnetizations (site CB-04 and CB-13 in their publication) with ages of 614 ± 16 and 623 ± 91 ka [*Frey et al., 2004*], respectively. Unaware of this study, we also sampled both of these flows. Our site EF corresponds to the exact sampling locality of site CB-04, and when revisiting the

locality, indeed, boreholes were found close by, covered by dense vegetation. Unfortunately, our ChRM directions were dispersed, preventing us from calculating a mean direction. An additional sampling in 2011 over a wider outcrop scale of >30 m showed that this locality apparently was widely exposed to lightning strikes, as samples had NRM intensities up to 125 A/m, Königsberger's ratios $Q=173$ in average, and dispersed NRM directions. In 7 out of 10 samples, AF demagnetization up to 80 mT removed most of the secondary components and approached a stable end direction. Therefore, we interpret that the characteristic direction of site EF indeed has a normal polarity, which could only be defined with a high uncertainty due to still unresolved characteristic magnetization directions (Table 2; $D=355.1^\circ$, $I=9.9^\circ$, $\alpha_{95}=15.9^\circ$, $n/N=7/10$, $P_{lat}=73.2^\circ$).

[44] Our site ED (Figure 12c) corresponds to site CB-13, but again no boreholes were found at the cited coordinates. We sampled five individual big blocks considered to be in situ cooling structures with 16 drill cores, resulting in a normal polarity mean direction (Figure 10c) of $D=358.6^\circ$, $I=17.3^\circ$, $\alpha_{95}=8.5^\circ$, $n/N=11/15$, $P_{lat}=77.6^\circ$. Thus, to confirm the excursions results of *Petronille et al.* [2005] once more, a resampling of both flows is required for both paleomagnetic and geochronology studies.

[45] 1. Site EN (671 ± 12 ka [*Lewis-Kenedi et al., 2005*]; Figure 13b) has a reversed polarity magnetization of $D=210.3^\circ$, $I=-33^\circ$, $\alpha_{95}=6.7^\circ$, $n/N=10/13$, $P_{lat}=-61.3^\circ$. This flow could have been emplaced during the Delta/Stage17 excursion first indicated by inclination lows found in a sediment core from Calabria, Southern Italy, by *Creer et al.* [1980]. *Biswas et al.* [1999] assigned intermediate to reversed directions to the Delta/Stage17 excursion occurring

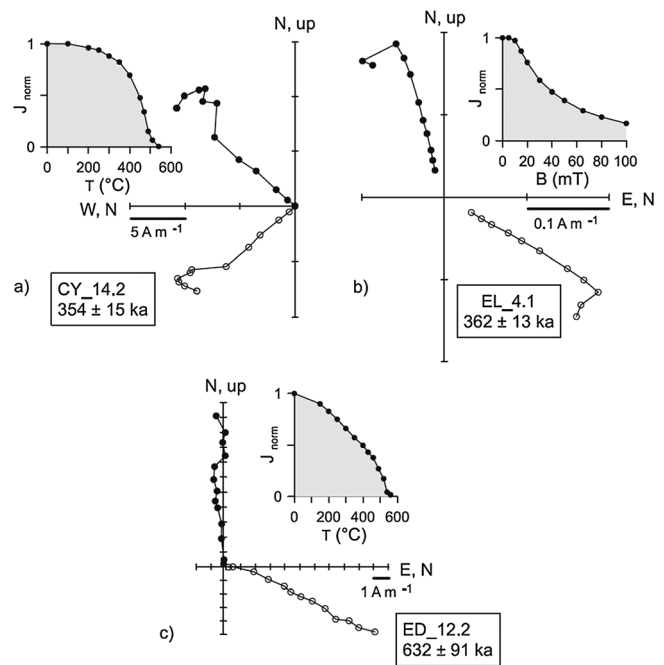


Figure 12. Orthogonal vector endpoint diagrams of demagnetization data from sites that yielded controversial results to previously published data. For definitions, see Figure 8.

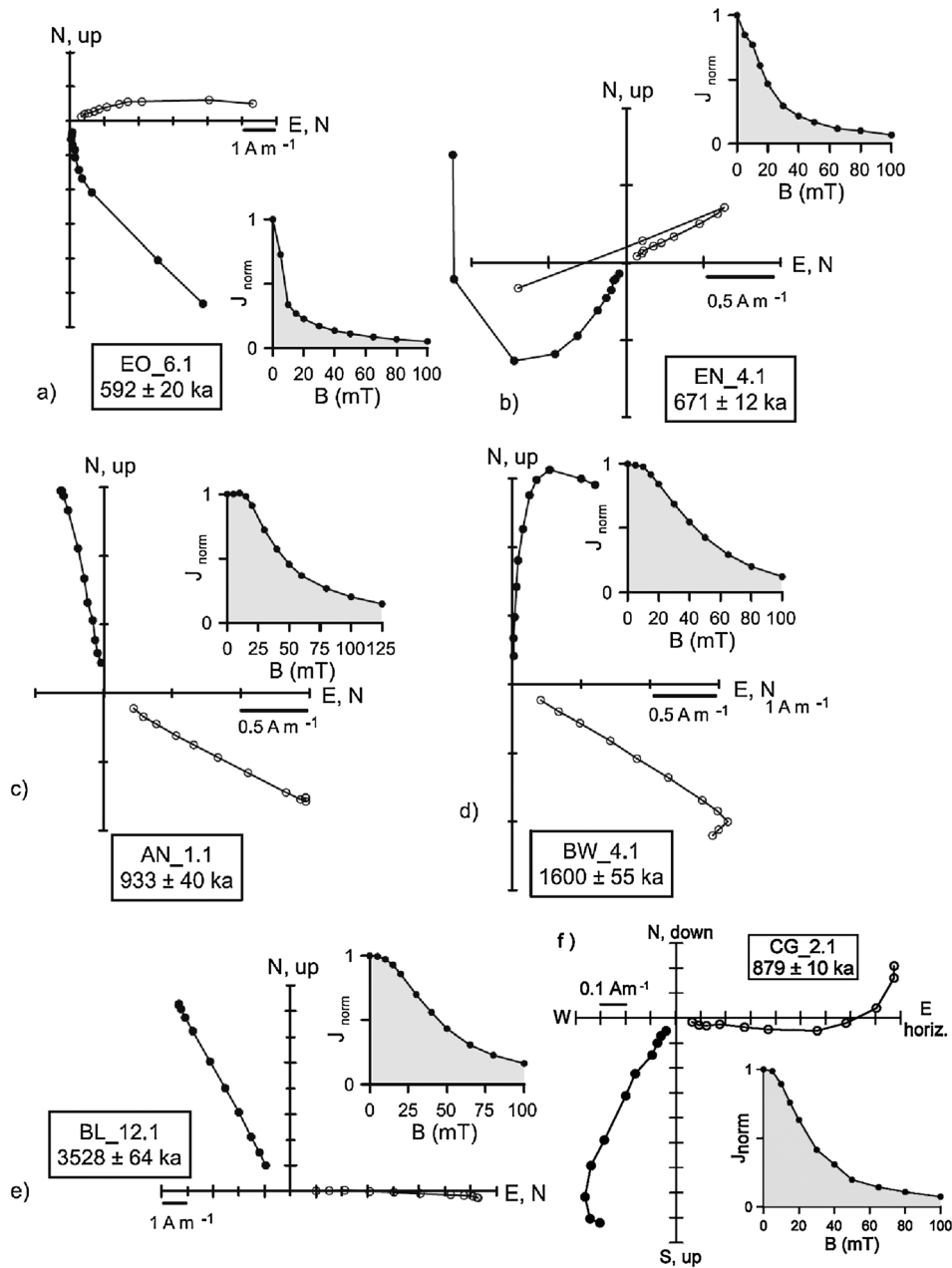


Figure 13. Orthogonal vector endpoint diagrams of demagnetization data from sites that are associated with geomagnetic excursions. For definitions, see Figure 8.

over about 7 ka at around 690 ka in a sediment core from the Osaka Basin, south-western Japan. However, as *Singer et al.* [2002] point out, the age of the Delta excursion requires further verification. There is evidence for the Delta/Stage17 excursion from sedimentary data obtained by *Channell et al.* [2004] who found inclination minima at around 665 ka in two astronomically dated cores (ODP sites 983 and 984) from the North Atlantic, Bjorn Drift/Iceland Basin. *Carcaillet et al.* [2004] reported a VDM (virtual dipole moment) minimum at around 700 ka in a ^{10}Be -derived VDM record from sedimentary records from the West Equatorial Pacific Ocean (North New Guinea). The first evidence that lava flow EN recorded the Delta/Stage17 excursion came from the study of *Ceja et al.* [2006]. They quoted an intermediate-reversed direction of $D=161.1^\circ$,

$I=21.4^\circ$, $\alpha_{95}=6.4^\circ$, $n/N=8/8$, $P_{\text{lat}}=-54.7^\circ$ (site TL-10 in their publication). We did not find their drill holes at their listed site coordinates, situated on top of a blocky lava flow. Our result is different from the previously published one and now indicates a fully reversed direction for this flow. As our drill cores definitely were recovered from the dated lava flow in a well-defined river cut about 200 m northeast of TL-10, where the flow was clearly unaffected by any post cooling movements, we propose our result to supersede that of *Ceja et al.* [2006]. We also note here that site EN is located only 560 m W of EO (see above) and at a ~ 60 m lower elevation. The reported age difference of ≈ 80 ka between the two flows may well correspond to their relative stratigraphic position, and future geochronology studies would have to show if they recorded recurrent excursions as observed by *Singer et al.*

[2008b] in the West Eifel volcanic field, or if rather the ages are not sufficiently well defined and the flows indeed recorded the same excursion.

[46] 2. Another site with an age indistinguishable from EN was sampled in the Michoacán-Guanajuato volcanic field at a distance of about 200 km, i.e., CG with 673 ± 10 ka [Ownby *et al.*, 2007]. It produced a reversed to intermediate direction of $D=231.3^\circ$, $I=-43.1^\circ$, $\alpha_{95}=11.8^\circ$, $n/N=9/11$, $P_{\text{lat}}=-42.9^\circ$ (Figure 12f). This direction is similar to that of flow EN, and both VGPs share similar longitudes of 166.8° and 150.9° and are roughly located between South Australia and Antarctica (Figure 10), suggesting that both flows indeed may have recorded the same geomagnetic excursion. The coincidence of geochronology ages and paleomagnetic record in two lava flows from different volcanic fields strongly supports that indeed both ages and reversed polarities are correct.

[47] Of all excursive lava flows mentioned above, only flow CG provided a paleo-intensity estimate: 33 ± 1 μT [Michalk *et al.*, 2010]. While this value is at the lower end of the reported paleo-intensities for the TMVB, the paleo-intensity is not as low as typically observed during geomagnetic excursions.

[48] All remaining Brunhes Chron sites provided normal polarity magnetizations. Site BV has an age of 882 ± 189 ka (this work), and the large error range overlaps with the upper Matuyama and lower Brunhes Chrons. The normal polarity observed in BV would suggest that this lava erupted during the Brunhes Chron. While it also could be correlated to some of the Matuyama excursions or the Jaramillo normal subchron, the large age error makes such correlations meaningless. Five lavas of normal polarity that based on the reported geochronology data are unambiguously assigned to the Matuyama Chron are discussed below.

[49] 1. Flow AN (949 ± 37 ka, this work; Figure 13c) has a normal polarity mean direction of $D=348.8^\circ$, $I=27.8^\circ$, $\alpha_{95}=8.3^\circ$, $n/N=10/12$, $P_{\text{lat}}=77.6^\circ$. According to its age, it could have been emplaced either during the Kamikatsura or the Santa Rosa excursion. The Kamikatsura excursion is constrained by Singer *et al.* [1999] to 900 ± 6 ka, based on $^{40}\text{Ar}/^{39}\text{Ar}$ ages from seven lavas with intermediate paleodirections from the Punaruu Valley (Tahiti), initially studied by Chauvin *et al.* [1990], and in lava flows from the Haleakala volcano (Hawaii), initially studied by Coe *et al.* [1985, 1995]. The Santa Rosa excursion is constrained by Singer and Brown [2002] to 936 ± 8 ka, based on $^{40}\text{Ar}/^{39}\text{Ar}$ ages obtained from the transitionally magnetized lavas from the Cerro San Rosa 1 rhyolite dome (New Mexico). Channell *et al.* [2002] identified a low in the relative paleo-intensity and VGP latitudes crossing the equator at ODP site 983 and suggest an age of 932 ka for the Santa Rosa excursion.

[50] 2. Flows DE (995 ± 120 ka, this work) and CN (1075 ± 34 ka) [Ownby *et al.*, 2007] have both normal magnetizations and were most likely emplaced during the worldwide recognized Jaramillo Normal Subchron, which had a duration of 68 ka, from 1001 to 1069 ka [Singer, 2007].

[51] 3. Flow AO (1095 ± 105 ka, this work) has a rather unusual direction of $D=3.8^\circ$, $I=-18.3^\circ$, $\alpha_{95}=6.2^\circ$, $n/N=8/10$, $P_{\text{lat}}=61.6^\circ$. However, assuming a cutoff angle of 40° , this direction would be still within the range of normal PSV values. Due to the rather large age error, this flow could

have been emplaced either during the younger part of the Jaramillo or during one of the two preceding normal polarity intervals, i.e., the Punaruu excursion or the Cobb Mountain Normal Subchron. Evidence for Punaruu excursion comes from normal to transitional magnetizations found in lavas from Punaruu Valley on the islands of Tahiti [Chauvin *et al.*, 1990] and later dated by Singer *et al.* [1999]. Singer [2007] quoted a recalibrated age of 1122 ± 10 ka for the Punaruu excursion. This excursion also appears in several sedimentary records where normal polarity magnetizations associated with relative paleo-intensity lows have been found around 1100 and 1115 ka [e.g., Guyodo *et al.*, 1999; Channell *et al.*, 2002]. The worldwide observed Cobb Mountain Normal Subchron is estimated to span the time interval from 1190 to 1215 ka [Channell *et al.*, 2002].

[52] 4. Flow BW (1628 ± 56 ka, this work; Figure 13d) has a normal polarity mean direction of $D=6.8^\circ$, $I=36.2^\circ$, $\alpha_{95}=9.2^\circ$, $n/N=11/14$, $P_{\text{lat}}=83.5^\circ$. Its age suggests that it was most likely emplaced during the Gilsa excursion, first studied by McDougall and Wensink [1966] and later by Watkins *et al.* [1975] in a section of a normal polarity lava with a K-Ar age of 1580 ka, overlying a normal polarity lava dated at 1670 ka in Iceland. Later, Clement and Kent [1987] presented new evidence for this excursion from sedimentary data from DSDP Site 609/North Atlantic and suggested an interpolated age of 1550 ka and duration of 8.8 ka. A similar duration of 8 ka (1567 to 1575 ka) for the Gilsa excursion is suggested, e.g., by Channell *et al.* [2002], based on marine sediments. In view of the large age error of ± 206 ka, BW could also correspond to an unnamed excursion around 1470 ka.

[53] 5. Flow BL (3528 ± 64 ka [Ownby *et al.*, 2011]; Figure 13e) has an anomalously flat inclination. The obtained mean direction of $D=334.8^\circ$, $I=1^\circ$, $\alpha_{95}=2.8^\circ$, $n/N=16/16$, $P_{\text{lat}}=59^\circ$ could therefore be interpreted as intermediate to normal, although the VGP latitude suggests normal PSV. According to its age, flow BL could have been emplaced during the C2An.3n subchron, which is estimated to span the time interval from 3330 to 3580 ka and which is recognized in the marine magnetic anomaly record [Cande and Kent, 1995].

8. Conclusions

[54] Paleosecular variation as estimated from the scatter of virtual geomagnetic poles of Pleistocene age lava flows from Mexico analyzed in this study gave similar values to those predicted by latitude-dependent Model G [McFadden *et al.*, 1988, 1991] and is also in agreement with high-quality Pleistocene paleomagnetic data from Mexico compiled by Mejia *et al.* [2005]. Paleomagnetic mean vectors of 57 lava flows were correlated to the Geomagnetic Polarity Timescale of Cande and Kent [1992, 1995] supplemented with data on geomagnetic excursions. This record revealed some further evidence for at least four, possibly five, geomagnetic excursions. We found that three lavas that erupted during the Brunhes Chron had nearly or fully reversed magnetizations. A flow dated at 592 ± 20 ka most likely erupted during the Big Lost excursion [Champion *et al.*, 1988; Singer *et al.*, 2002, Singer, 2007]. Two flows dated at 671 ± 13 and 679 ± 10 ka give new evidence for the Delta/Stage 17 excursion [Creer *et al.*, 1980; Biswas *et al.*,

1999]. These flows are from different volcanic fields and provide independent evidence strongly suggesting that both geochronology and paleomagnetic data are reliable and that these flows indeed recorded a geomagnetic event. Finally, seven lava flows that erupted during the Matuyama chron were found to have recorded normal polarity magnetizations. From these, a flow dated at 949 ± 37 ka was correlated to the Santa Rosa excursion [Singer and Brown, 2002]. Another flow dated at 1628 ± 56 ka most likely erupted during the Gilsa excursion [McDougall and Wensink, 1966]. Furthermore, a lava flow of Pliocene age, dated at 3528 ± 54 ka, has a normal to intermediate direction and was most likely emplaced during subchron C2An.3n [Cande and Kent, 1995].

[55] This study also revealed some findings in conflict with previously published data by Petronille *et al.* [2005] and Ceja *et al.* [2006]. Two lava flows interpreted by Ceja *et al.* [2006] to have intermediate directions and associated with the Levantine excursion (354 ± 15 and 362 ± 13 ka) [Ryan, 1972] were found to have normal polarity magnetizations within the range of usual PSV. Another flow dated at 623 ± 91 ka with a reversed polarity magnetization that was correlated to the Big Lost excursion by Petronille *et al.* [2005] was found to have a normal polarity magnetization. This highlights the importance for multiple verification of such results before adopting them in the Geomagnetic Instability Timescale of Singer *et al.* [2002, 2008a, 2008b; Singer, 2007]. We verified at least twice the field localities and site coordinates to assure that we indeed sampled the dated lava flows, and we are confident about the quality of our paleomagnetic results. But no repeat geochronology studies have been carried out so far to also confirm the age of any of those rocks.

[56] The most important outcome of our geomagnetic investigation is the finding of nearly fully reversed polarity magnetizations in three Brunhes Chron lavas, with VGP's deviating 135° or more from the geographic North Pole. The only cryptochron included in the geomagnetic polarity timescale of Cande and Kent [1992, 1995] in the Brunhes Chron is C1n-1, which spans the interval from 493 to 504 ka. Two flows with reversed polarity magnetizations found in this study do not fall into that time window and would thus correspond to a different and new cryptochron around 670–680 ka.

[57] **Acknowledgments.** The constructive revision of Brad Singer and Mats Knudsen (of previous versions), Klaudia Kuiper, and anonymous reviewers is acknowledged. We would like to thank D. Berger, G. Arnold, and M. Köhler (GFZ) for their help in the sample preparation. J. Herwig (GFZ) is thanked for her assistance during backscattered electron microscope studies. Much appreciated assistance during fieldwork came from I. Barajas and G. Gonzalez (Centro de Geociencias, Queretaro). M.A. García, A.S. Rosas, L.C. Gradilla, V. Pérez, and G. Rendón (CICESE) participated in different aspects of the ^{40}Ar - ^{39}Ar experiments. This research was funded by DFG grants Ne154/45-1, No334/1-2, and No334/5-1, Conacyt grant 46213, and PAPIIT-UNAM grant IN114606.

References

Aguirre-Díaz, G. J. (1996), Volcanic stratigraphy of the Amealco caldera and vicinity, Central Mexican Volcanic Belt, *Revista Mexicana de Ciencias Geológicas*, *13*, 10–51.
 Aguirre-Díaz, G. J., L. Ferrari, S. A. Nelson, G. Carrasco-Núñez, M. López-Martínez, and J. Urrutia-Fucugauchi (1998), El Cinturón Volcánico Mexicano: Un Nuevo Proyecto Multidisciplinario, *Unión Geofísica Mexicana, Geos*, *18*(2), 131–138.

Aguirre-Díaz, G. J., M.C. Jaimes-Viera, and J. Nieto-Obregón (2006), The Valle de Bravo volcanic field. Geology and geomorphometric parameters of a Quaternary monogenic field at the front of the Mexican Volcanic Belt, in *Neogene-Quaternary Continental Margin Volcanism: A Perspective From Mexico*, edited by Siebe, C., J.L. Macías, and G.J. Aguirre-Díaz, *Geol. Soc. Amer. Spec. Paper*, *402*, 125–140.
 Biswas, D. K., M. Hyodo, Y. Taniguchi, M. Kaneko, S. Katoh, H. Sato, Y. Kinugasa, and K. Mizuno (1999), Magnetostratigraphy of Pliocene-Pleistocene sediments in a 1700-m core from Osaka Bay, southwestern Japan and short geomagnetic events in the middle Matuyama and early Brunhes Chrons, *Paleogeography, Paleoclimatology, Paleocology*, *148*, 233–248.
 Blatter, D. L., I. S. E. Carmichael, A. L. Deino, and P. R. Renne (2001), Neogene volcanism at the front of the central Mexican volcanic belt: Basaltic andesites to dacites, with contemporaneous shoshonites and high-TiO₂ lava, *Geol. Soc. Amer. Bull.*, *113*(10), 1324–1342.
 Bloemendal, J., J. W. King, F. R. Hall, and S.-J. Doh (1992), Rock magnetism of late Neogene and Pleistocene deep-sea sediments: Relationship to sediment source, diagenetic processes, and sediment lithology, *J. Geophys. Res.*, *97*, 4361–4375.
 Böhnell, H., and R. Molina-Garza (2002), Secular variation in Mexico during the last 40,000 years, *Phys. Earth Planet. Inter.*, *133*, 99–109.
 Böhnell, H., and J. F. W. Negendank (1981), Preliminary results of paleomagnetic measurements of Tertiary and Quaternary igneous rocks from the eastern part of the Trans Mexican volcanic belt, *Geofis. Int.*, *20*, 235–248.
 Böhnell, H., N. Reismann, G. Jäger, U. Haverkamp, J. F. W. Negendank, and H.-U. Schmincke (1987), Paleomagnetic investigation of Quaternary West Eifel volcanics (Germany): Indication for increased volcanic activity during geomagnetic excursion/event?, *J. Geophys.*, *62*, 50–61.
 Böhnell, H., D. Michalk, N. Nowaczyk, and G. Gonzalez Naranjo (2009), The use of mini-samples in paleomagnetism, *Geophys. J. Int.*, *179*, 35–42.
 Brunhes, B. (1906), Recherches sur le direction d'aimantation des roches volcaniques, *J. Phys.*, *5*, 705–724.
 Cande, S. C., and D. V. Kent (1992), A new geomagnetic polarity time scale for the Late Cretaceous and Cenozoic, *J. Geophys. Res.*, *97*, 13,917–13,951.
 Cande, S. C., and D. V. Kent (1995), Revised calibration of the geomagnetic polarity timescale for the Late Cretaceous and Cenozoic, *J. Geophys. Res.*, *100*, 6093–6095.
 Carcaillet, J.T., D.L. Bourles, and N. Touveny (2004), Geomagnetic dipole moment and ^{10}Be production rate intercalibration from authigenic $^{10}\text{Be}/^{9}\text{Be}$ for the last 1.3 Ma. *Geochem. Geophys. Geosyst.*, *5*, Q05006, doi:10.1029/2003GC000641.
 Carrasco-Núñez, G., M. Ort, and C. Romero (2007), Evolution and hydrological conditions of a maar volcano (Atexcac crater, Eastern Mexico), *J. Volcanol. Geotherm. Res.*, *159*, 179–197.
 Carrasco-Núñez, G., L. Siebert, R. Díaz-Castellón, L. Vázquez-Selem, and L. Capra (2010), Evolution and hazard of a long-quietest compound shield-like volcano: Cofre de Perote, Eastern Trans-Mexican Volcanic Belt, *J. Volcanol. Geotherm. Res.*, *197*, 209–224.
 Ceja, M. R., A. Goguitchaichvili, M. Calvo-Rathert, J. Morales-Contreras, L. Alva-Valdivia, J. R. Elguera, J. Urrutia-Fucugauchi, and H. D. Granados (2006), Paleomagnetism of the Pleistocene Tequila volcanic field (Western Mexico), *Earth Planets Space*, *58*, 1349–1358.
 Champion, D. E., M. A. Lanphere, and M. A. Kuntz (1988), Evidence for a new geomagnetic reversal from lava flows in Idaho: Discussion of short polarity reversals in the Brunhes and late Matuyama Polarity Chrons, *J. Geophys. Res.*, *93*, 11,667–11,680.
 Channell, J. E. T., A. Mazaud, P. Sullivan, S. Turner, and M.E. Raymo (2002), Geomagnetic excursions and paleointensities in the Matuyama Chron at Ocean Drilling Program sites 983 and 984 (Iceland Basin). *J. Geophys. Res.*, *107*(B6), 2114, doi:10.1029/2001JB000491.
 Channell, J. E. T., J. H. Curtis, and B. P. Flower (2004), The Matuyama-Brunhes boundary interval (500–900 ka) in North Atlantic drift sediments, *Geophys. J. Int.*, *158*, 489–505.
 Chauvin, A., P. Roperch, and R. A. Duncan (1990), Records of geomagnetic reversals from volcanic islands of French Polynesia. 2. Paleomagnetic study of a flow sequence (1.2 to 0.6 Ma) from the Island of Tahiti and discussion of reversal models, *J. Geophys. Res.*, *95*, 2727–2752.
 Clement, B. M. (2004), Dependence of duration of geomagnetic polarity reversals on site latitude, *Nature*, *428*, 637–640.
 Clement, B. M., and D. V. Kent (1987), Short polarity intervals within the Matuyama: Transitional field records from hydraulic piston cored sediments from the North Atlantic, *Earth Planet. Sci. Lett.*, *81*, 253–264.
 Coe, R. S., V. Hsu, and F. Theyer (1985), Matuyama-Brunhes record from Maui: Transitional directions, *Eos. Trans. AGU*, *66*, 872.
 Coe, R. S., M.S. Pringle, and B.S. Singer (1995), Haleakala transition zone may be a concatenation. *Eos. Trans. AGU*, *76*(46), Fall Meet. Suppl., Abstract F176.

- Coe, R. S., B. S. Singer, M. S. Pringle, and X. Zhao (2004), Matuyama-Brunhes reversal and Kamikatsura event on Maui: Paleomagnetic directions, $^{40}\text{Ar}/^{39}\text{Ar}$ ages and implications, *Earth Planet. Sci. Lett.*, *222*, 667–684.
- Conte, G., J. Urrutia-Fucugauchi, A. Goguitchaichvili, and J. Morales (2006), Low-latitude paleosecular variation and the time-averaged field during the late Pliocene and Quaternary—Paleomagnetic study of the Michoacan-Guanajuato volcanic field, Central Mexico, *Earth Planets Space*, *58*, 1359–1371.
- Cox, A. (1969), Confidence limits for the precision parameter k , *Geophys. J. R. astr. Soc.*, *18*, 545–549.
- Creer, K. M., P. W. Readman, and A. M. Jacobs (1980), Paleomagnetic and paleontological dating of a section at Gioia Tauro, Italy: Identification of the Blake event, *Earth Planet. Sci. Lett.*, *50*, 289–300.
- Day, R., M. Fuller, and V. A. Schmidt (1977), Hysteresis properties of titanomagnetites: Grain-size and compositional dependence, *Phys. Earth Planet. Inter.*, *13*, 260–267.
- Demant, A. (1978), Características del Eje Neovolcánico Transmexicano y sus problemas de interpretación, *Revista Mexicana de Ciencias Geológicas*, *2*, 172–182.
- Doell, R. R., and A. V. Cox (1972), The Pacific geomagnetic secular variation anomaly and the question of lateral uniformity in the lower mantle. in *The Nature of the Solid Earth*, edited by E. C. Robinson, pp. 245–284, McGraw-Hill, New York.
- Dunlop, D. J. (2002), Theory and application of the Day plot (Mrs/Ms versus Hcr/Hc) 1. Theoretical curves and tests using titanomagnetite data. *J. Geophys. Res.*, *107*(B3), 2056, doi:10.1029/2001JB000486.
- Fisher, R. A. (1953), Dispersion on a sphere, *Proc. R. Soc. London*, *217*, 295–305.
- Frey, H., R. A. Lange, C. M. Hall, and H. Delgado-Granados (2004), Magma eruption rates constrained by $^{40}\text{Ar}/^{39}\text{Ar}$ chronology and GIS for the Ceboruco–San Pedro volcanic field, western Mexico, *Geol. Soc. Amer. Bull.*, *116*, 259–276.
- Gonzalez, S., G. Sherwood, H. Böhnell, and E. Schnepf (1997), Paleosecular variation in Central Mexico over the last 30 000 years: The record from lavas, *Geophys. J. Int.*, *130*, 201–219.
- Gubbins, D. (1999), The distinction between geomagnetic excursions and reversals, *Geophys. J. Int.*, *137*, F1–F3.
- Guyodo, Y., and J.-P. Valet (1999), Global changes in intensity of the Earth's magnetic field during the last 800 kyr, *Nature*, *399*, 249–252.
- Guyodo, Y., C. Richter, and J.-P. Valet (1999), Paleointensity record from Pleistocene sediments (1.4–0 Ma) off the California Margin, *J. Geophys. Res.*, *104*, 22953–22964.
- Haggerty, S. E. (1991), Oxide textures—A mini-atlas, oxide minerals: Petrologic and magnetic significance, *Rev. Miner.*, *25*, 129–219.
- Herrero-Bervera, E., and S. Pal (1977), Paleomagnetic study of Sierra de Chichinautzin, Mexico, *Geofis. Int.*, *17*, 167–180.
- Herrero-Bervera, E., J. Urrutia-Fucugauchi, A. L. Martin del Pozzo, H. N. Böhnell, and J. Guerrero (1986), Normal amplitude Brunhes paleosecular variation at low latitudes: A paleomagnetic record from the Trans-Mexican Volcanic Belt, *Geophys. Res. Lett.*, *13*, 1442–1445.
- Hoffman, K. A., and B. S. Singer (2004), Regionally recurrent paleomagnetic transitional fields and mantle processes, in *Timescales of the Paleomagnetic Field*, *Amer. Geophys. Union, Geophys. Monogr. Ser. 145*, edited by J. E. T. Channell, D. V. Kent, W. Lowrie, and J. G. Meert, pp. 233–243, AGU, Washington D. C.
- Johnson, C. L., et al. (2008), Recent investigations of the 0–5 Ma geomagnetic field recorded by lava flows. *Geochem. Geophys. Geosyst.*, *9*(4), Q04032, doi:10.1029/2007GC001696.
- Kirschvink, J. L. (1980), The least-squares line and plane and the analysis of paleomagnetic data, *Geophys. J. Roy. Astron. Soc.*, *62*, 699–718.
- Klitgord, K. D., and J. Mammerickx (1982), Northern East Pacific Rise—Magnetic anomaly and bathymetric framework, *J. Geophys. Res.*, *87*, 6725–6783.
- Knudsen, M. F., G. M. Henderson, C. M. Mac Niocaill, and A. J. West (2007), Seven thousand year duration for a geomagnetic excursion constrained by $^{230}\text{Th}_{\text{ex}}$, *Geophys. Res. Lett.*, *34*, L22302, doi:10.1029/2007GL031090.
- Krásá, D., and J. Matzka (2007), Inversion of titanomagnetite in oceanic basalt during heating, *Phys. Earth planet. Inter.*, *160*, 169–179.
- Langereis, C. G., M. J. Dekkers, G. J. De Lange, M. Pateme, and P. J. M. Van Santvoort (1997), Magnetostratigraphy and astronomical calibration of the Last 1.1 Myr from an eastern Mediterranean piston core and dating of short events in the Brunhes, *Geophys. J. Int.*, *129*, 75–94.
- Lawrence, K., C. G. Constable, and C. L. Johnson (2006), Paleosecular variation and the average geomagnetic field at $\pm 20^\circ$ latitude. *Geochem. Geophys. Geosyst.*, *7*, Q07007, doi:10.1029/2005GC001181.
- Lewis-Kenedi, C. B., R. A. Lange, C. M. Hall, and H. Delgado-Granados (2005), The eruptive history of the Tequila volcanic field, western Mexico: Ages, volumes, and relative proportions of lava types, *Bull. Volcanol.*, *67*, 391–414.
- Lund, S. P., G. Acton, B. Clement, M. Hastedt, M. Okada, and T. Williams (1998), Geomagnetic field excursions occurred often during the last million years, *Eos. Trans. AGU*, *79*, 178–179.
- Lund, S., J. S. Stoner, J. E. T. Channell, and G. Acton (2006), A summary of Brunhes paleomagnetic field variability recorded in Ocean Drilling Program cores, *Phys. Earth Planet. Inter.*, *ODP Contributions to Paleomagnetism*, *156*, 194–204.
- McDougall, I., and H. Wensink (1966), Paleomagnetism and geochronology of the Pliocene-Pleistocene lavas in Iceland, *Earth Planet. Sci. Lett.*, *1*, 232–236.
- McElhinny, M. W., and P. L. McFadden (1997), Paleosecular variation over the past 5 Myr based on a new generalized database, *Geophys. J. Int.*, *131*, 240–252.
- McFadden, P. L., R. T. Merrill, and M. W. McElhinny (1988), Dipole/quadrupole family modeling of paleosecular variation, *J. Geophys. Res.*, *93*, 11,583–11,588.
- McFadden, P. L., R. T. Merrill, M. W. McElhinny, and S. Lee (1991), Reversals of the Earth's magnetic field and temporal variations of the dynamo families, *J. Geophys. Res.*, *96*, 3923–3933.
- Mejía, V., H. Böhnell, N. D. Opdyke, M. A. Ortega-Rivera, J. K. W. Lee, and J. J. Aranda-Gomez (2005), Paleosecular variation and time-averaged field as recorded in lavas flows from Mexico, *Geochem. Geophys. Geosyst.*, *6*, doi:10.1029/2004GC000871.
- Merrill, R. T., and P. L. McFadden (1994), Geomagnetic field stability: Reversal events and excursions, *Earth Planet. Sci. Lett.*, *121*, 57–69.
- Michalk, D. M., A. J. Biggin, M. F. Knudsen, H. N. Böhnell, N. R. Nowaczyk, S. Ownby, and M. López-Martínez (2010), Application of the multispecimen palaeointensity method to Pleistocene lava flows from the Trans-Mexican Volcanic Belt, *Phys. Earth Planet. Inter.*, *179*, 139–156.
- Michalk, D. M., A. R. Muxworthy, H. N. Böhnell, I. MacLennan, and N. Nowaczyk (2008), Evaluation of the multispecimen parallel differential pTRM method: A test on historical lavas from Iceland and Mexico, *Geophys. J. Int.*, *173*, 409–420.
- Mooser, F., A. E. M. Nairn, and J. F. W. Negendank (1974), Paleomagnetic investigations of the Tertiary and Quaternary igneous rocks: VIII. A paleomagnetic and petrologic study of volcanics of the Valley of Mexico, *Geol. Rundsch.*, *63*, 451–483.
- Morales, J., A. Goguitchaichvili, and J. Urrutia-Fucugauchi (2001), A rock-magnetic and paleointensity study of some Mexican volcanic lava flows during the Latest Pleistocene to the Holocene, *Earth Planets Space*, *53*, 893–902.
- Moskowitz, B. M. (1981), Methods for estimating Curie temperatures of titanomagnetites from experimental Js-T data, *Earth Planet. Sci. Lett.*, *53*, 84–88.
- Nowaczyk, N. R., and T. W. Frederichs (1999), Geomagnetic events and relative paleointensity variations during the past 300 ka as recorded in Kolbeinsey Ridge Sediments, Iceland Sea: Indication for a strongly variable geomagnetic field, *Int. J. Earth Sci.*, *88*, 116–131.
- Nowaczyk, N. R., and J. Knies (2000), Magnetostratigraphic results from Eastern Arctic Ocean—AMS14C ages and relative paleointensity data of the Mono Lake and Laschamp geomagnetic events, *Geophys. J. Int.*, *140*, 185–197.
- O'Reilly, W. (1984), *Rock and Mineral Magnetism*, Blackie, Glasgow and London; Chapman and Hall, New York, pp. 220.
- Opdyke, N. D. (1972), Paleomagnetism of deep-sea cores, *Rev. Geophys. Space Phys.*, *10*, 213–249.
- Ort, M. H., and G. Carrasco-Núñez (2009), Lateral vent migration during phreatomagmatic and magmatic eruptions at Tecuitlapa Maar, east-central Mexico, *J. Volcanol. Geotherm. Res.*, *181*, 67–77.
- Ownby, S., H. Delgado Granados, R. A. Lange, and C. M. Hall (2007), Volcán Tancitaro, Michoacán, Mexico, $^{40}\text{Ar}/^{39}\text{Ar}$ constraints on its history of sector collapse, *J. Volcan. Geoth. Res.*, *161*, 1–14.
- Ownby, S. E., R. A. Lange, C. M. Hall, and H. Delgado-Granados (2011), Origin of andesite in the deep crust and eruption rates in the Tancitaro-Nueva Italia region of the central Mexican arc, *Geol. Soc. Amer. Bull.*, *123*, 274–294.
- Petronille, M., A. Goguitchaichvili, B. Henry, L. M. Alva-Valdivia, J. Rosas-Elguera, J. Urrutia-Fucugauchi, M. Rodríguez Ceja, and M. Calvo-Rathert (2005), Paleomagnetism of Ar-Ar dated lava flows from the Ceboruco-San Pedro volcanic field (western Mexico): Evidence for the Matuyama-Brunhes transition precursor and a fully reversed geomagnetic event in the Brunhes chron. *J. Geophys. Res.*, *110*, B08101, doi:10.1029/2004JB003321.
- Renne, P. R., C. C. Swisher, A. L. Deino, D. B. Karner, T. L. Owens, and D. J. DePaolo (1998), Inter-calibration of standards, absolute ages and uncertainties in $^{40}\text{Ar}/^{39}\text{Ar}$ dating, *Chem. Geol.*, *145*, 117–152.
- Ruiz-Martínez, V. C., M. L. Osete, R. Vegas, J. I. Nunez-Aguilar, J. Urrutia-Fucugauchi, and D. H. Tarling (2000), Paleomagnetism of late Miocene to Quaternary volcanics from the eastern segment of the Trans-Mexican volcanic belt, *Tectonophysics*, *318*, 217–233.

- Ryan, W. B. (1972), Stratigraphy of late Quaternary sediments in the eastern Mediterranean, in *The Mediterranean Sea*, edited by D. J. Stanley, pp. 149–169, Dowden, Hutchinson & Ross, Stroudsburg.
- Schaaf, P., and A. Ramirez-Luna (2008), Advancement in luminescence dating of volcanic rocks: Examples from the Eastern Trans-Mexican Volcanic Belt, *IAVCEI, General Assembly*, Reykjavik, August 2008, abstracts.
- Schnepf, E. (1994), Determination of paleointensities from the Quaternary West Eifel volcanic field, Germany, *Geophys. J. Int.*, *116*, 688–714.
- Schnepf, E., and H. Hradetzky (1994), Combined paleointensity and $^{40}\text{Ar}/^{39}\text{Ar}$ age spectrum data from volcanic rocks of the West Eifel field (Germany): Evidence for an early Brunhes geomagnetic excursion, *J. Geophys. Res.*, *99*, 9061–9076.
- Schwarz, W. H., and M. Trieloff (2007), Intercalibration of $^{40}\text{Ar}/^{39}\text{Ar}$ age standards NL-25, HB3gr hornblende, GA 1550, SB-3, HD-B1 biotite and BMus/2 muscovite, *Chem. Geol.*, *242*, 218–231.
- Singer, B. S. (2007), Polarity transitions: Radioscopic dating, in *Encyclopedia of Geomagnetism and Paleomagnetism* edited by D. Gubbins, and E. Herrero-Bervera, pp. 834–839, Springer, Dordrecht, The Netherlands.
- Singer, B. S., and L. L. Brown (2002), The Santa Rosa event: $^{40}\text{Ar}/^{39}\text{Ar}$ and paleomagnetic results from the Valles rhyolite near Jaramillo Creek, Jemez Mountains, New Mexico, *Earth Planet. Sci. Lett.*, *197*, 51–64.
- Singer, B. S., K. A. Hoffman, A. Chauvin, R. S. Coe, and M. S. Pringle (1999), Dating transitionally magnetized lavas of the late Matuyama Chron: Toward a new $^{40}\text{Ar}/^{39}\text{Ar}$ timescale of reversals and events, *J. Geophys. Res.*, *104*, 679–693.
- Singer, B. S., M. K. Relle, K. A. Hoffman, A. Battle, C. Laj, H. Guillou, and J. C. Carracedo (2002), Ar/Ar ages from transitionally magnetized lavas on La Palma, Canary Islands, and the geomagnetic instability timescale, *J. Geophys. Res.*, *107*(B11), 2307, doi:10.1029/2001JB001613.
- Singer, B. S., L. L. Brown, J. O. Rabassa, and H. Guillou (2004), $^{40}\text{Ar}/^{39}\text{Ar}$ chronology of late Pliocene and Early Pleistocene geomagnetic and glacial events in southern Argentina, in *Timescales of the Paleomagnetic Field*, *Geophys. Monogr. Ser.*, vol. 145, edited by J. E. T. Channell et al., pp. 175–190, AGU, Washington, D. C.
- Singer, B. S., K. A. Hoffman, R. S. Coe, L. L. Brown, B. R. Jicha, M. S. Pringle, and A. Chauvin (2005), Structural and temporal requirements for geomagnetic field reversal deduced from lava flows, *Nature*, *434*, 633–636.
- Singer, B. S., B. R. Jicha, B. T. Kirby, J. W. Geissman, and E. Herrero-Bervera (2008a), $^{40}\text{Ar}/^{39}\text{Ar}$ dating links Albuquerque Volcanoes to the Pringle Falls excursion and the geomagnetic instability time scale, *Earth Planet. Sci. Lett.*, *267*, 584–595.
- Singer, B. S., K. Hoffmann, E. Schnepf, and H. Guillou (2008b), Multiple Brunhes Chron excursions recorded in West Eifel (Germany) volcanics: Support for long-held mantle control over the non-axial dipole field, *Phys. Planet. Int.*, *169*, 28–40.
- Steele, W. K. (1985), Paleomagnetic constraints on the volcanic history of Iztaccihuatl, *Geofis. Int.*, *24*, 159–167.
- Steiger, R. H., and E. Jäger (1977), Subcommittee on geochronology: Convention on the use of decay constants in geo- and cosmochronology, *Earth Planet. Sci. Lett.*, *36*, 359–362.
- Tauxe, L., and D. V. Kent (2004), A simplified statistical model for the geomagnetic field and the detection of shallow bias in paleomagnetic inclinations: Was the ancient magnetic field dipolar? Timescales of the paleomagnetic field, *Geophysical Monograph Series*, *145*, 101–115.
- Tauxe, L., T. A. T. Mullender, and T. Pick (1996), Potbellies, wasp-waists, and superparamagnetism in magnetic hysteresis, *J. Geophys. Res.*, *101*, 571–583.
- Tauxe, L., H. Staudigel, and J. R. Wijbrans (2000), Paleomagnetism and $^{40}\text{Ar}/^{39}\text{Ar}$ ages from La Palma in the Canary Islands, *Geochem. Geophys. Geosyst.*, *1*(9), doi:10.1029/2000GC000063.
- Urrutia-Fucugauchi, J., C. Radakrishnamurthy, and J. F. W. Negendank (1984), Magnetic properties of a columnar basalt from central Mexico, *Geophys. Res. Lett.*, *9*, 832–835.
- Vandamme, D. (1994), A new method to determine paleosecular variation, *Phys. Earth Planet. Inter.*, *85*, 131–142.
- Watkins, N. D., L. Kristjansson, and I. McDougall (1975), A detailed paleomagnetic survey of the type location for the Gilsa geomagnetic polarity event, *Earth Planet. Sci. Lett.*, *27*, 436–444.
- Wicht, J. (2005), Paleomagnetic interpretation of dynamo simulations, *Geophys. J. Int.*, *162*, 371–380.
- York, D., N. M. Evensen, M. López Martínez, and J. De Basabe Delgado (2004), Unified equations for the slope, intercept, and standard errors of the best straight line, *Am. J. Phys.*, *72*, 367–375.